ENHANCEMENT OF MICROSTRIP ANTENNAS AND TRANSMISSION LINES PERFORMANCE USING PBG

By

Mehran Fallah-Rad

A Thesis
submitted to the Faculty of Graduate Studies
in partial fulfillment of the requirements
for the degree of

Master of Science

Department of Electrical and Computer Engineering
The University of Manitoba

THE UNIVERSITY OF MANITOBA

FACULTY OF GRADUATE STUDIES

*****

COPYRIGHT PERMISSION PAGE

EHHANCEMENT OF MICROSTRIP ANTENNAS AND TRANSMISSION LINES PERFORMANCE USING PBG

BY

MEHRAN FALLAH-RAD

A Thesis/Practicum submitted to the Faculty of Graduate Studies of The University of Manitoba in partial fulfillment of the requirements of the degree of

Master of Science

Dedicated to my parents, who have
taught me the true value of knowledge and
instilled in me the ambition to excel

Acknowledgments

I would like to express my appreciation and gratitude to my advisor, Prof. L. Shafai for his advise, encouragement, and insight throughout my research. The work presented in this thesis would not have been possible without his guidance and support.

I would also like to acknowledge the valuable and constructive suggestions provided by Dr. G. Bridges. His advice as one of my committee members was greatly appreciated. Special thanks to Dr. N. Sepehri for serving in my committee as well. Moreover, I would like to extend a special thanks to Mr. B. Tabachnick for his technical assistance, and to Ms. S. Girardin for her help whenever it was needed.

Finally, I would like to thank my parents and my sister for their continuous support and understanding. Their endless love and moral support has helped me in completing this degree and achieving my goals in life.

Abstract

This thesis is an investigation of two dimensional photonic bandgap structures (i.e. PBG's) and their applications in microstrip antennas and transmission lines. The photonic bandgap structures under study are ground plane PBG's and high impedance PBG's. The ground plane PBG's consist of perforations in the ground plane of microstrip structures. The perforations are placed in the ground plane of narrowband and wideband antennas as well as microstrip transmission lines. The overall effect of the ground plane perforations on the gain, bandwidth, resonant frequency and, the radiation pattern of the antennas are studied. For narrowband microstrip antennas, the perforations are used to prevent the excitation of the higher order modes while, for the wideband antennas the perforations are used to increase the bandwidth of the antennas. In the case of the microstrip transmission lines, the ground plane perforations are modified in order to create a wideband filter from the transmission line structure. The effective epsilon values are then calculated using a Matlab program for each filter structure. In addition to the ground plane PBG's, a second type of PBG consisting of metal patches with shorting vias (i.e. High Impedance PBG) is also investigated. The high impedance PBG is used in the design of the patch antennas on different dielectric structures. The effect of the PBG on the gain, radiation pattern, resonant frequency and, bandwidth of the antennas is studied. Each structure in the study is simulated using the commercial software Ansoft Ensemble which, is based on the method of moments (MoM). For seven cases the structures are fabricated and tested at the Antenna Laboratory at the University of Manitoba. For the fabricated cases the measured results are compared with the simulation data.

Table of Contents

List of Figures

List of Tables

Chapter 1

Introduction

1.1 Preface

Microstrips are printed circuits for very high frequency electronics and microwaves [1]. Physically, any microstrip structure consists of a thin plate of low-loss insulating material called the substrate covered with metal completely on one side (i.e. Ground plane) and partly on the other side where the circuit or antenna patterns are printed [1]. The printed elements could be transmission lines, couplers, filters, antennas etc. The structures under study in this thesis are the microstrip transmission lines and microstrip patch antennas.

The microstrip antenna is a type of open wave guiding structure consisting of a radiating patch on one side of a dielectric substrate and a ground plane on the other side [2]. Microstrips are known for their advantages in terms of lightweight, low volume, low cost, and compatibility with integrated circuits. These advantages make this antenna a very useful candidate in applications such as mobile radio, satellite communications, radar, biomedical radiators and feed elements in reflectors. The printed antennas come in many shapes such as square, rectangular, circular, triangular, elliptical and more complex geometry's as the radiating elements [1]. As one might expect, there are certain disadvantages to these structures such as the narrow bandwidth, losses due to surface waves, radiation from the surface waves, polarization impurities and, low power handling capabilities. These have led to a new multidisciplinary field of study called the "Photonic bandgap" structures (i.e. PBG's). These are periodic structures in 1, 2, or 3 dimensions

which can stop the propagation of electromagnetic waves in certain directions for certain frequencies. PBG's are characterized by the type of symmetries, the dielectric contrast between the constituent materials, and by the shape and period of the structure.

PBG's come in many shapes and forms such as holes drilled through the dielectric, patterns etched in the ground plane of microstrips and, metallic patches placed around the microstrip structures. It has been shown that by the use of PBG's in microstrips, one can change their properties completely. For instance, the etching of holes underneath a transmission line structure would create a filter with a stopband related to the size and spacing of the etched patterns in the ground [3]. In the case of microstrip patch antennas, the etching of holes can lead to prevention of excitation of higher order modes [4]. Without the use of PBG, this would typically be done using more than one feed element which would make the design more complicated.

In addition, it has been reported that the use of PBG in patch antennas will improve the antenna efficiency, reduce the sidelobe and backlobe radiation levels and, increase the antenna gain by suppressing the surface waves [5-10].

Ground plane perforations have previously been used in microstrip transmission lines and microstrip patch antennas. However, no information has been provided on the effective dielectric constants of these structures in any publications.

In general, the use of PBG ground planes has not been fully explored and requires further investigation to better understand the basic properties of these structures.

In the case of high impedance PBG's, the structures have only been tested on high dielectric constant materials. However, they have not been used on materials with low permittivities. In addition, there is a common belief that the PBG structures prevent the

flow of surface waves and thereby increase the gain of the antenna. In this thesis this property is further investigated. It is shown that, in contrast to the common belief, the increase in the gain increase is due to a combination of different factors and not the cancelation of the surface waves alone. Thus, by use of proper combination of parameters, one can increase the gain of an antenna by as much as 3 to 4 times.

1.2 Thesis Objectives

The objective of this thesis is to study the properties of two different PBG structures and their effects on the performance of microstrip patch antennas and microstrip transmission lines. The effects of PBG on the bandwidth, gain, resonant frequency and radiation patterns of different antennas are investigated. A new type of wide band filter with very low isolation levels is designed using the ground plane PBG structure. In addition, an increase in the effective epsilon of the filter structure is found by Matlab simulations and experimentally. The effects of the ground plane perforations on narrowband and wideband microstrip patch antennas are also investigated. For the narrowband patch antennas, it is found that by using the right combination of ground plane perforations (i.e. Holes or slots in the ground plane) a shift in the resonance of higher order modes or prevention of the excitation of the higher modes can be achieved. For the case of a wideband antenna, an increase in the bandwidth of the structure is obtained using slots in the ground plane.

In addition to the ground plane PBG's, the properties of high impedance PBG structures around microstrip antennas are also studied in detail. The bandgap of the structures on

different substrate materials are found by placing an incident wave on the PBG structure and looking at the radar cross section (i.e. RCS) of the PBG. Once the bandgaps are found, the PBG's are placed around patch antennas and their effects on the performance of patch antennas are investigated. By selection of proper PBG structures, improvements in the gain and radiation patterns of patch antennas on low dielectric constant materials are achieved. Finally, seven different antennas with PBG structures are fabricated and tested in the Antenna Laboratory at the University of Manitoba. The experimental results are then compared with the simulations.

1.3 Thesis Outline

This thesis is divided into several chapters. The first chapter covered the introduction to microstrips and photonic bandgap structures along with the objectives of the thesis. The second chapter covers the basic background theory on microstrip structures, namely microstrip transmission lines and microstrip patch antennas. The basic formulas used in the design of transmission lines and patch antennas are given. In addition, the basics of photonic bandgap structures are explained and their applications in microstrips are discussed. The third chapter covers the microstrip transmission lines with ground plane perforations. The effects of perforations in the ground plane of transmission lines are studied along with the effective permittivities of such structures.

Chapter four covers the microstrip patch antennas with ground plane perforations. The effects of perforations in the ground plane of narrowband and wideband patch antennas are studied. The ground perforations include a single hole, multiple holes and slots in the

ground plane. The use of perforations in the ground to control the modes in patch antennas are studied in detail.

Chapter five covers the high impedance photonic bandgap structures and their applications in microstrip patch antennas. The basic properties of high impedance PBG's are explained along with the technique used to measure the bandgap of the structures. The structures are used in the design of microstrip patch antennas on different substrate materials. The dielectric materials used have dielectric constants ranging from 1.0 to 9.8. The properties of the PBG on each dielectric material along with the effects on the gain, radiation patterns and the resonant frequency of the antennas are studied.

Chapter six covers the measurement results obtained from the fabricated antennas. The measured data from the fabricated antennas are compared with the simulated data obtained from the simulation software. Finally, chapter seven provides a conclusion on the work done along with suggestions for future work.

Chapter 2

Background Theory

In this chapter, the basic background theory on microstrip patch antennas and microstrip transmission lines are reviewed. The equations for calculating the resonant frequency, input impedance, gain, effective epsilon and other parameters are discussed. In addition, a summary of different two dimensional photonic bandgap structures and their applications in microstrip circuits is given.

2.1 Microstrip Structures

This section is divided into two parts. The first part covers the microstrip transmission lines and their properties while the second part covers the microstrip patch antennas.

2.1.1 Microstrip Transmission Lines

A transmission line is made of two or more conducting strips or wires along which electrical signals propagate ideally without attenuation [1]. This is under the condition that the conductor and the dielectric material used are lossless. The microstrip transmission line is one of the most popular types of planar transmission lines primarily because it can be fabricated by photolithographic processes, and is easily integrated with other passive and active microwave devices [11]. The geometry of a microstrip tline is shown in Fig. 2.1a. The structure in the figure consists of a transmission line of width W on a substrate of permittivity ε_r and thickness of d. As it can be seen from Fig. 2.1b, the fields in a microstrip transmission line are not confined within the dielectric only. Some

of the field lines are in the air region above the substrate. As a result, the dielectric constant will be combination of the dielectric constant of air and that of the substrate. This is called the effective permittivity and is given by [11]:

$$\epsilon_e = \frac{(\epsilon_r + 1)}{2} + \frac{(\epsilon_r - 1)}{2}\left(1 + \frac{12h}{W}\right)^{\frac{-1}{2}} \qquad 1 < \epsilon_e < \epsilon_r \qquad (2.1)$$

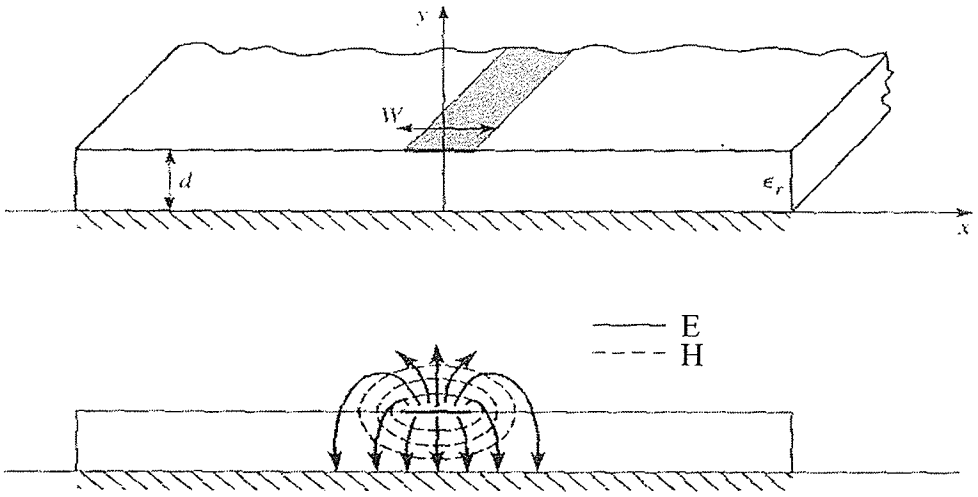

Fig. 2.1 Geometry of a transmission line (a) Top view
(b) Cross sectional view of the field lines

From equation 2.1 the effective dielectric constant can be found based on the substrate thickness and width of the transmission line. Another important property of a microstrip transmission line is its characteristic impedance. The characteristic impedance of a transmission line is given by [11]:

$$Z_o = \frac{60}{\sqrt{(\epsilon_e)}} \ln\left(\frac{8d}{W} + \frac{W}{4d}\right) \qquad \frac{W}{d} \leq 1 \qquad (2.2-a)$$

$$Z_o = \frac{(120\pi)}{\left(\sqrt{(\epsilon_e)}\left[\frac{W}{d} + 1.393 + 0.667 \ln\left(\frac{W}{d} + 1.444\right)\right]\right)} \qquad \frac{W}{d} \geq 1 \qquad (2.2-b)$$

Given the dimensions of the microstrip line, its characteristic impedance can be calculated from the above equations.

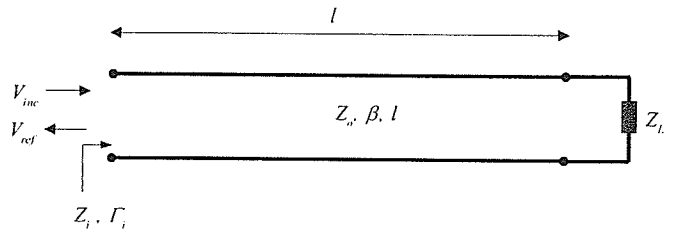

Fig. 2.2 Geometry of a lossless transmission line connected to a load impedance Z_L

Figure 2.2 shows a lossless transmission line of length l that is connected to a load impedance Z_L. The input impedance of the above transmission line is given by [11]:

$$Z_i = Z_o \frac{[Z_L + jZ_o \tan\beta l]}{[Z_o + jZ_L \tan\beta l]} \qquad (2.3)$$

Given the load impedance Z_L, the characteristic impedance Z_o, the wave number β and the length of the transmission line l, one can find the input impedance from the above equation. The input impedance is a very important parameter in the design of any structure. Typically the input impedance should be 50 Ω in order to get a perfect match with other structures such as the source. In any other case a matching circuit would be

added to the input of the transmission line in order to get an input impedance that would match the transmission line to the source or any other device that is connected at the input.

From the input impedance one can find the reflection coefficient which is the ratio of the reflected wave over the incident wave at the input. The reflection coefficient in terms of the input impedance is given by [11]:

$$\Gamma = \frac{(Z_i - Z_o)}{(Z_i + Z_o)} \tag{2.4}$$

where Z_i is the input impedance of the line and Z_o is the characteristic impedance of the structure that is connected to the input of the transmission line. The reflection coefficient has a maximum magnitude of one and a minimum of zero in the case of a perfectly matched line.

2.1.2 Microstrip Patch Antennas

The microstrip patch antenna is a type of open wave guiding structure, which consists of a radiating patch on one side of a dielectric and a ground plane on the other side [2]. Microstrip antennas come in many shapes such as rectangular, circular, elliptical, triangular and many others. Linear and circular polarizations can be achieved by using a single patch or multiple patches in the form of an array. In this section, the rectangular microstrip patch antenna is discussed along with the necessary equations for the design of the patch.

The geometry of a square microstrip patch antenna is shown in Fig. 2.3. This a patch with length L and width W that is linearly polarized in the y direction. At the first

resonance, this structure behaves as a one dimensional resonator with a length equal to half wavelength at the resonant frequency. Different types of feed structures are used in microstrip antennas. The geometry in Fig. 2.3 shows a probe fed patch antenna. Other feeding methods include transmission line feed and slot coupling feed. Each feeding technique has it's own advantages and disadvantages and the selection of one will be based on the design requirements of the antenna.

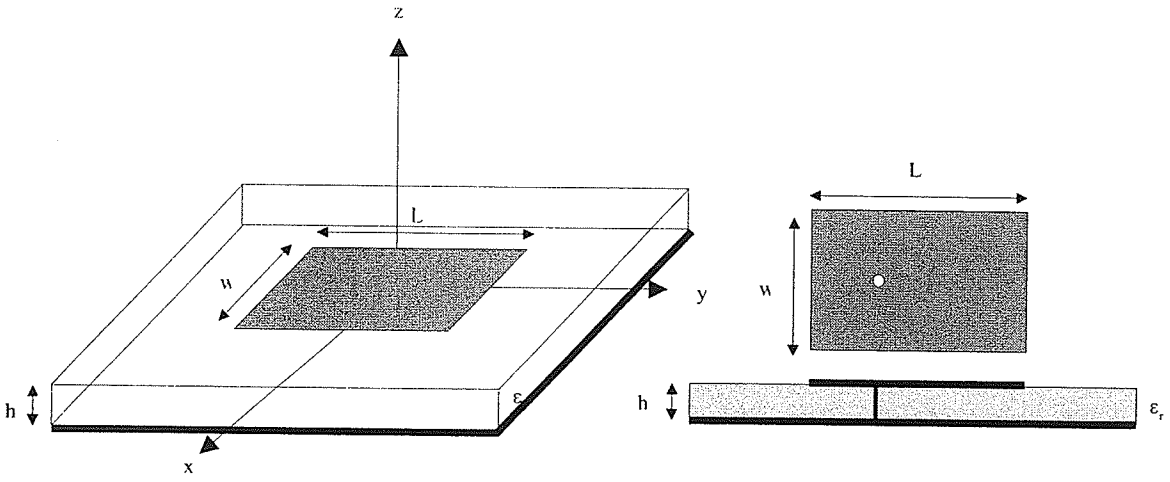

Fig. 2.3 Geometry of a rectangular microstrip patch antenna

Fig. 2.4 shows the side view of the patch antenna. The vertical lines are the electric field underneath the patch. For a small height, the electric field under the patch is normal to the patch. Due to the fringing of electric field at the patch edges, the length of the patch is increased by $2\Delta L$. This is known as the effective length of the patch ($L_e = L + 2\Delta L$).

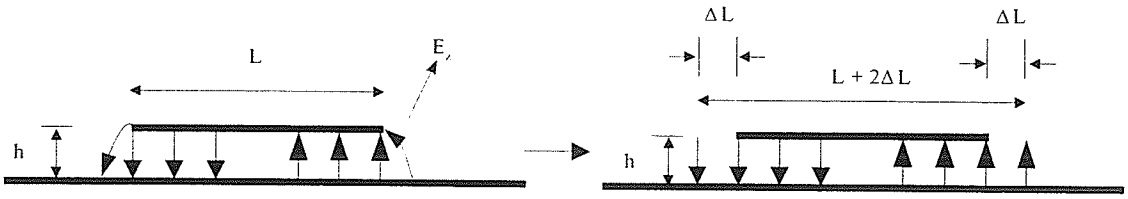

Fig. 2.4 Sideview of a patch antenna with the fringing fields

The increment (ΔL) can be found from [16]:

$$\Delta L = 0.412\,h \frac{[(\epsilon_e + 0.3)(\frac{W}{h} + 0.264)]}{[(\epsilon_e - 0.258)(\frac{W}{h} + 0.8)]} \qquad (2.5)$$

Next is the resonant frequency of a patch which is dependent on the effective permittivity and the effective length of the patch as shown below [16].

$$f_r = \frac{C}{(2(L + 2\Delta L)\sqrt{(\epsilon_e)})} \qquad (2.6)$$

This is the frequency of the dominant mode that is excited by placing the feed along the patch length. In addition to the dominant mode, there are other modes that are excited at higher frequencies. The resonant frequency of these modes can be found from [16]:

$$f_r = \frac{C}{(2\pi\sqrt{\epsilon_e})}\sqrt{[(m\frac{\pi}{a})^2 + (n\frac{\pi}{b})^2]} \qquad (2.7)$$

Each specific mode has it's own current distribution on the patch and hence it's own radiation pattern. The excitation of higher order modes can be prevented by using multiple feeds or by using PBG structures as will be shown in the following chapters.

As mentioned previously the electric field underneath the patch is normal to the patch and

different for each particular mode. The electric field underneath the patch is given by [16]:

$$E_z = \frac{V_o}{h} \cos(m\pi \frac{x}{L}) \cos(n\pi \frac{y}{W}) \qquad (2.8)$$

where V_o is the voltage applied between the patch and the ground plane. By using the cavity model and aperture theory one can find the far field radiation equations of a patch antenna [17].

Another important parameter of a microstrip patch antenna is it's bandwidth of operation. The bandwidth of operation is typically defined as the range of frequencies for which certain requirements are satisfied. For instance, for the reflection coefficient bandwidth is usually defined as the range of frequencies for which the reflection coefficient is below -10 dB. The bandwidth of a microstrip patch antenna can be expressed in terms of it's quality factor and the voltage standing wave ratio. The quality factor is a figure of merit that is representative of the antenna losses [12]. The quality factor is given by:

$$\frac{1}{Q_{tot}} = \frac{1}{Q_{rad}} + \frac{1}{Q_c} + \frac{1}{Q_d} + \frac{1}{Q_{sw}} \qquad (2.9)$$

where the total quality factor is defined in terms of the radiation quality factor, conduction quality factor, dielectric quality factor and surface waves quality factor. The bandwidth of the antenna is defined by [12]:

$$BW = \frac{(VSWR - 1)}{(Q_{tot}\sqrt{(VSWR)})} \qquad (2.10)$$

Finally, the directivity of a patch antenna is another important parameter to consider. The directivity is given as the ratio of the radiation intensity in a given direction from the antenna to the radiation intensity averaged over all directions.

$$D = \frac{(4\pi U)}{P_{rad}} \qquad (2.11)$$

where U is the radiation intensity in a given direction. The maximum directivity can also be found approximately by [12]:

$$D_o = \frac{41253}{(\Theta_{1d}\Theta_{2d})} \qquad (2.12)$$

where Θ_{1d} and Θ_{2d} are the half power beamwidths in two orthogonal planes.

2.2 Photonic Bandgap Structures:

Photonic bandgap structures are periodic structures in 1, 2 or 3 dimensions that stop the propagation of electromagnetic waves in certain directions for certain frequencies. These structures come in many shapes and forms and their properties depend on the geometry, type of symmetry, dimensions, and the constituent material. The use of PBGs range from optical frequencies to microwave and millimeter wave applications. In optical region the PBGs could be used to guide photons much like a waveguide in microwave frequencies. In the microwave and millimeter wave region, the PBGs have been used in the design of antennas, filters, waveguides, amplifiers, and phase shifters [5-10]. In this thesis we are primarily interested in the applications of two dimensional PBGs in the design of microstrip structures (i.e. Microstrip patch antennas and microstrip transmission lines).

In most cases, the PBGs have been used to "so-call" eliminate the propagation of the

surface waves generated by the antenna, thereby reducing the negative effects associated with them. Surface waves are present in many situations involving microstrip antennas. They occur at the interface between the metal and free space and decay exponentially into the surrounding materials [10]. Once surface waves are generated, they propagate until they reach bends or discontinuities where they diffract and radiate into free space (Fig. 2.5). The radiation at the discontinuities, causes interference with the main radiation from the antenna and can be seen in form of ripples in the pattern. By using PBGs, the propagation of surfaces waves are prevented leading to higher gains and overall smoother radiation patterns.

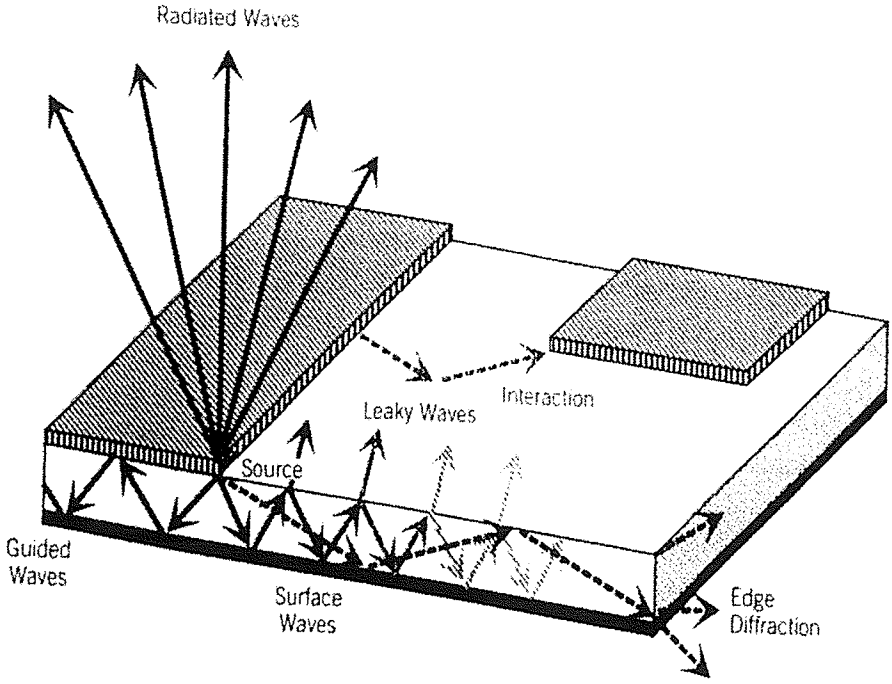

Fig. 2.5 Propagation of surface waves in a microstrip structure [1]

The PBGs used in microstrip patch structures can be categorized into three main groups. The first group are the dielectric PBGs in which the dielectric material used in the design of an antenna has been modified by drilling holes in the substrate. The holes can be one, two or three dimensional periodic patterns of different shapes, periodicity, and material. The refractive index of the etched holes, and the shape and the period of the lattice will define the electromagnetic properties of the dielectric. An example of a patch antenna with a dielectric PBG is shown in Fig. 2.6. As it can be seen, the geometry consists of circular columns of air with period d and diameter of 2r drilled through the dielectric. Dielectric PBGs have been used in patch antennas to enhance the gain, reduce the sidelobe and backlobe radiation levels and decrease the ripples in the overall pattern [5].

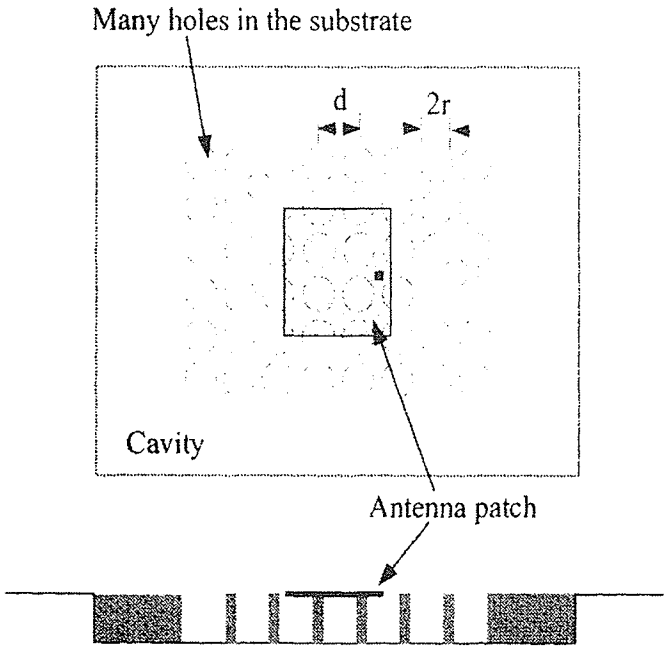

Fig. 2.6 Geometry of a patch antenna placed on a dielectric PBG

Next are the ground plane PBGs which, consist of periodic patterns etched in the ground plane of microstrip structures. The ground plane PBGs have mainly been used in microstrip transmission lines to create filters with stopbands related to the period of the PBG [3]. The geometry of two different types of ground plane PBGs are shown in Fig. 2.7a and 2.7b. The geometry in part (a) is a transmission line with circular holes etched in the ground. The geometry of Fig. 2.7b is another PBG structure also referred to as a Uniplanar Compact Photonic Bandgap (UC-PBG) structure which will be discussed later. The period of the PBGs shown in Fig. 2.6 and Fig. 2.7 (i.e. a) are related to the center frequency of the stopband of the filter by [3,7]:

$$a = \frac{c}{(2f_{center}\sqrt{(\epsilon_e)})} \qquad (2.13)$$

where ε_e is the effective permittivity of the structure. Therefore, by knowing the center frequency of the stopband, the period of the structure can be calculated using equation 2.13. The bandwidth of the filter stopband is determined by other parameters, which are different for both structures shown above. For the structure with circular holes in the ground, the bandwidth of the stopband increases with the enlargement of the circular holes. Ground plane perforations have also been used in the design of microstrip patch antennas to prevent the excitation of higher order modes [4]. The geometry of a patch antenna with a PBG ground plane is shown in Fig. 2.8. The use of ground plane perforations will be studied in more detail in the next chapter.

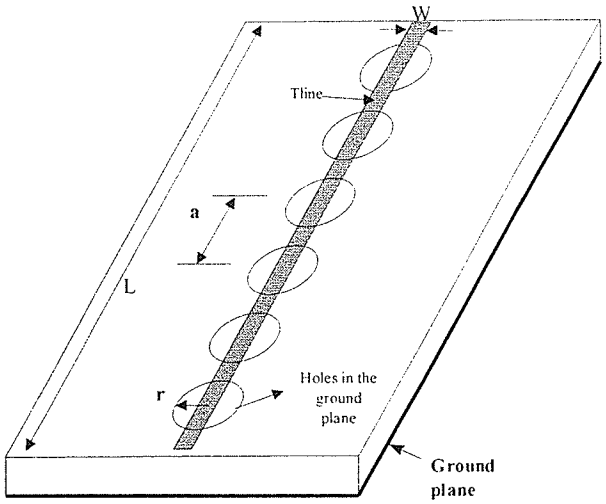

(a)

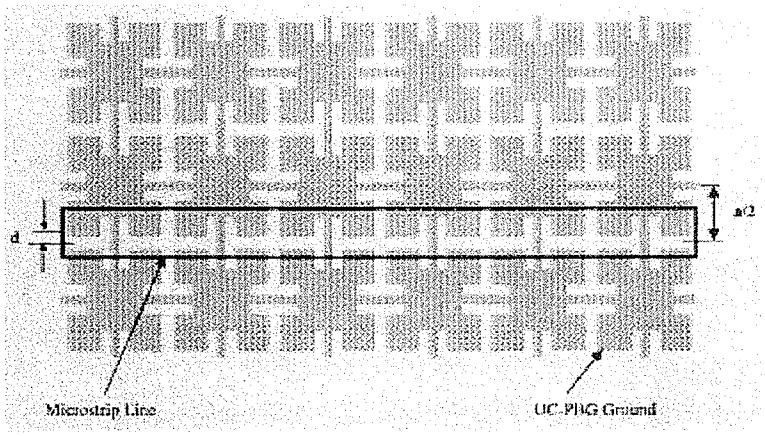

(b)

Fig. 2.7 (a) A ground plane PBG using circular holes (b) UC-PBG ground plane [7]

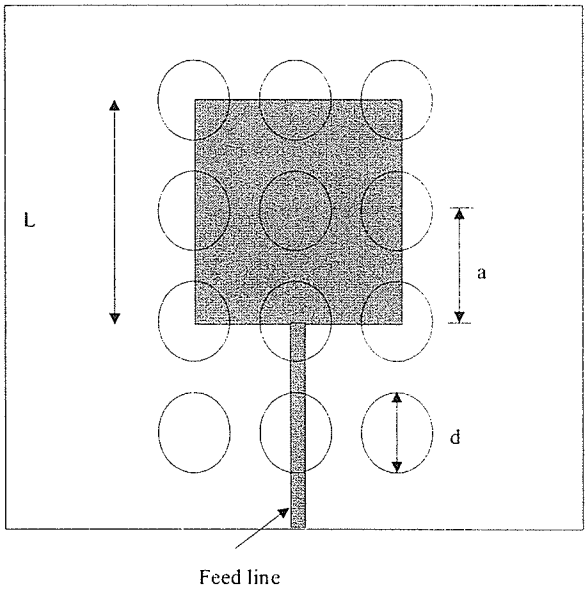

Fig. 2.8 Geometry of a patch antenna with PBG ground plane

The last type of PBG used in microstrip structures consists of metal patches placed on top of the dielectric adjacent to the microstrips. The PBGs in this group can be categorized in to two types. The first type contains metal patches that are joined to one another with connecting branches (i.e. UC-PBG) as shown in Fig. 2.7(b). Each element of the PBG lattices consists of square metal pads with four connecting branches. The connecting branches introduce inductance's while the adjacent pads with gaps in between introduce large capacitance's forming a distributed LC network [7]. There is a bandgap associated with this structure where the propagation of the TM and TE surface waves are prohibited. This bandgap would depend on the dimensions of the PBG and the type of the substrate material used. UC-PBG structures have been used in the design of patch antennas to improve the gain and the radiation pattern of the antenna [12-13].

The second type of PBGs with metal patches behaves similarly to a UC-PBG except for the fact that the patches are not connected to one another and instead they are shorted to the ground plane using vias (Fig. 2.9).

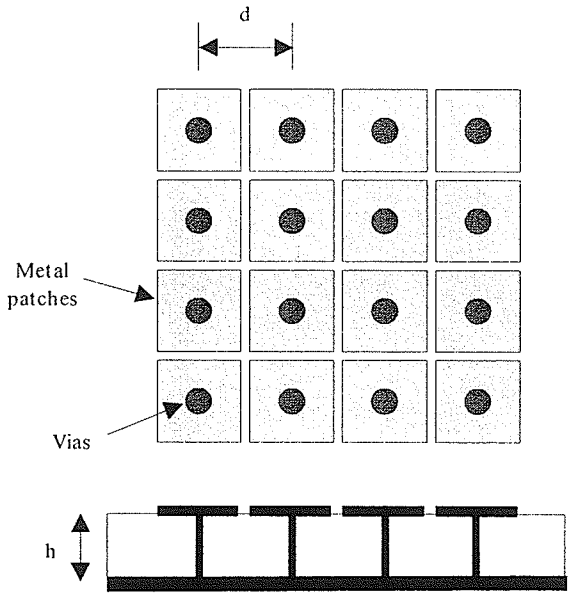

Fig. 2.9 Geometry of the High Impedance PBG

The grounding vias in this case introduce inductance's while the adjacent patches create capacitance's. If the period of surface texture is much smaller than the wavelength, the structure can be described using an effective medium model and it's qualities can be summarized into it's surface impedance [10]. The surface impedance of the metal surface described here is characterized by an equivalent parallel resonant LC circuit given by:

$$Z = \frac{(j\omega L)}{(1-\omega^2 LC)} \qquad (2.14)$$

where the resonant frequency of such a circuit is given by:

$$\omega_o = \frac{1}{\sqrt{(LC)}} \qquad (2.15)$$

At the resonant frequency the surface impedance becomes very high and this is associated with the band gap of the structure [10]. Looking at equation 2.15, one can control the resonance of the structure by changing the capacitance and inductance values. The capacitance can be controlled by changing the dimensions of the square patches and the spacing between the adjacent patches while the inductance can be controlled by changing the diameter and length of the vias. The inductance and capacitance values for a particular structure can be solved for numerically using the proper simulation tools.

The above structure has been used in the design of microstrip patch antennas to improve the gain and radiation patterns of the patch. This structure will be studied in more detail in the following chapters.

2.3 Conclusion

This chapter covered the basics of microstrip transmission lines and microstrip patch antennas. The fundamental formulas necessary for the design of microstrips such as the input impedance, characteristic impedance, resonant frequency, and directivity were given. Next, the basics of photonic bandgap structures were introduced. Different PBG structures and their applications in microstrip transmission lines and microstrip patch antennas were reviewed. It was explained that by the use of specific PBG structures in the ground plane of microstrip transmission lines, a filter can be created with properties related to the period and dimensions of the PBG. Additionally, the use of PBGs in microstrip patch antennas increased the gain and efficiency of the patch and provided an overall smoother radiation patterns.

Chapter 3

Microstrip Transmission Lines with Ground Plane Perforations

This chapter covers the microstrip transmission lines on perforated ground planes and is divided into 3 sections. The first section covers the narrowband PBG filters and their properties. The second section covers a new type of wideband PBG filter along with simulation results. In the last section, the effective epsilon values for the filter structures obtained from simulation and measurements are compared and discussed.

3.1 Narrowband PBG Filter

In the previous chapter it was mentioned that by replacing the ground plane of a transmission line with a PBG structure, we can create a filter with a stopband center frequency related to the period of the PBG. The period of the PBG is equal to half wavelength at the center frequency of the stopband, Eq. 2.13. The geometry of Fig. 3.1 shows a transmission line of width W and length L that is placed on a PBG ground plane. The holes in the ground plane have a radius r and a center to center spacing of a also defined as the period of the structure. The stopband bandwidth of this filter is related to the diameter of circular holes, the larger the hole diameter, the wider the stopband bandwidth. The use of circular holes in the ground plane of a transmission line has been previously investigated by Radisic and Qian [3]. However, their design makes use of 3 columns of circular holes. Since the fringing of the fields occurs in the vicinity of the

transmission line, the use of 3 columns of holes becomes unnecessary as will be shown later on.

In order to better understand the behavior of the structure in Fig. 3.1, simulations were done using Ansoft Ensemble simulator which, is based on the method of moments (MoM). All the filters in this chapter, simulated and fabricated, are designed on a substrate material with a permittivity of 3.2 and a substrate thickness of 1.59 mm.

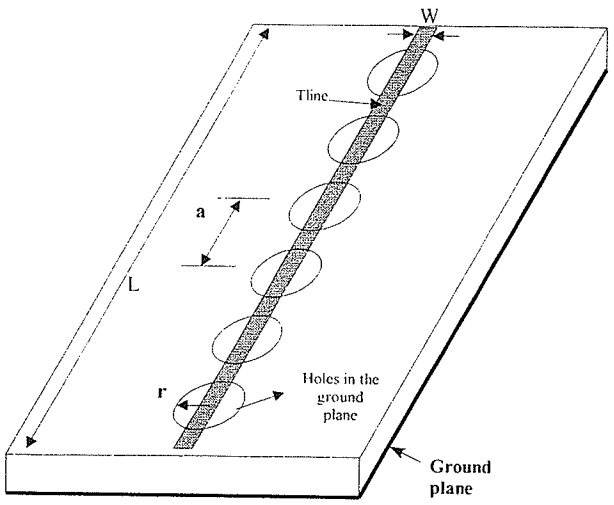

Fig. 3.1 Geometry of a PBG filter

In order to see the effects of hole diameter on the stopband bandwidth, a filter with a length of 102 mm and width of 4 mm corresponding to a 50 Ω line was simulated in Ensemble. The period of the holes is 13 mm corresponding to a stopband center frequency of 7.4 GHz and a total of 6 holes is used under the transmission line. The transmission coefficient, i.e. S_{21}, of the filter for different hole diameters is shown in Fig. 3.2. As it can be seen from the S_{21} plots, the hole diameter has a significant effect on the bandwidth of the filter. It should also be noted that the stopband of the filter repeats at an

integer multiples of the center stop frequency. In addition, there is a limit on the diameter of holes before the filter properties are changed.

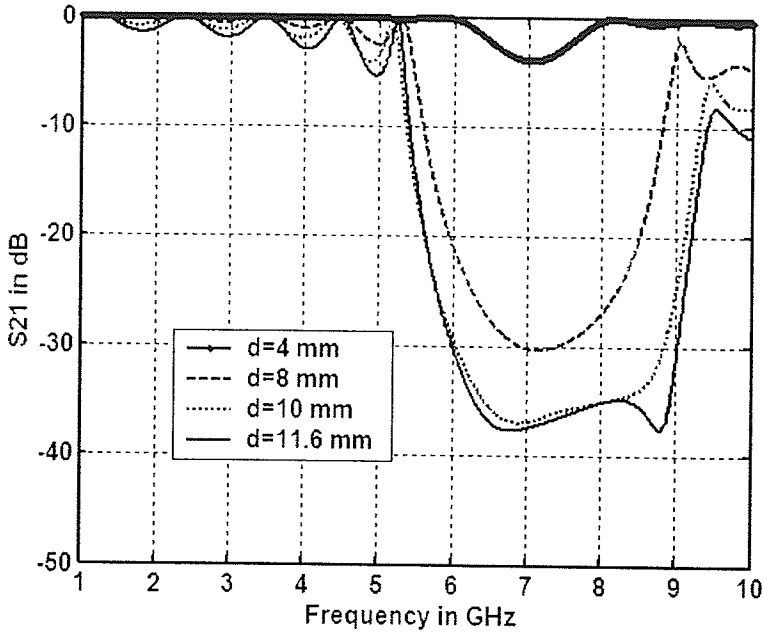

Fig. 3.2 Plots of S_{21} vs. frequency for different hole diameters
L = 102 mm, W = 4mm, h = 1.59 mm, ε_r = 3.2

Next, simulations were done in order to compare the effects of one and three columns of holes in the ground. Fig. 3.3 shows the S_{21} of a filter with one and three columns of holes. For this case the diameter of the holes is 10 mm and the remaining dimensions are the same as the filter in Fig. 3.2 . As it can be seen form Fig. 3.3, not much difference exists between the two cases. Therefore, one column of holes would be sufficient enough to create a filter out of the transmission line. In addition to the circular holes, other geometry's were also tested for comparison. 10 mm × 10 mm square pattern of holes in the ground plane were used and compared with 10 mm diameter circular holes. The S_{21} for the square holes and the circular holes are plotted in Fig. 3.4. The S_{21} of the two structures are slightly shifted, and this is due to the fact that the square holes in the

ground have a larger physical area than the circular holes. However, both structures provide a wide stopband at the desired frequency of 7.4 GHz.

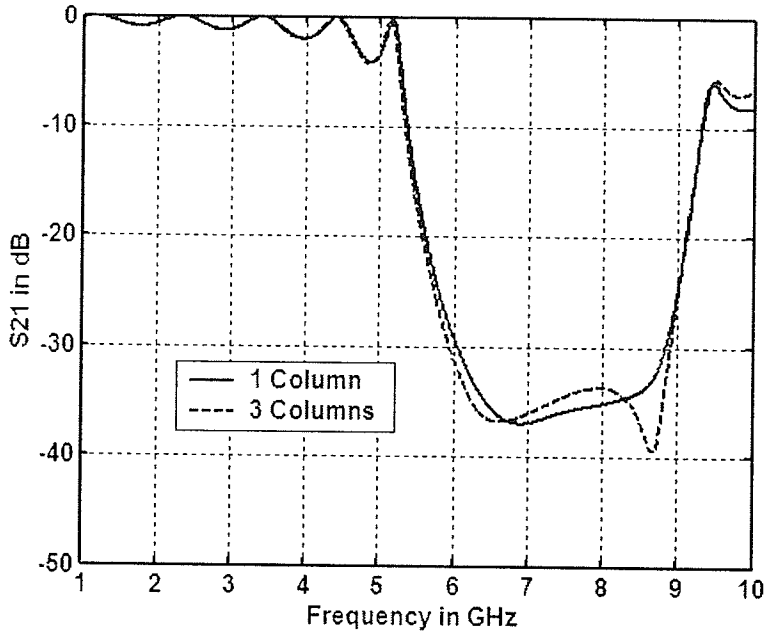

Fig. 3.3 Comparison of a filter with a single column and 3 columns of holes in the ground plane

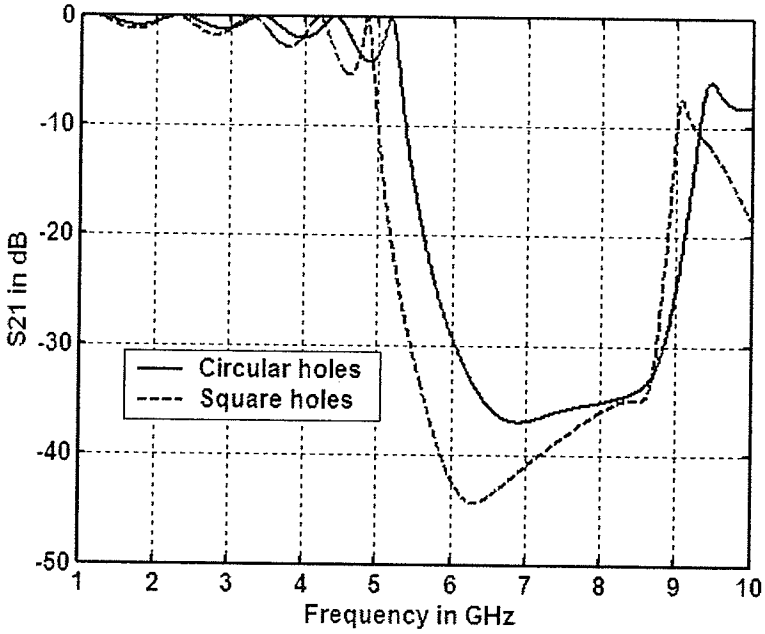

Fig. 3.4 Comparison of a filter with 10 mm diameter circular holes and 10mm × 10 mm square holes in the ground plane

In order to verify the results obtained from Ensemble, the filter in Fig. 3.2 with circular holes of diameter 11.6 mm was fabricated and tested. The resulting S_{21} parameter obtained from the network analyzer is compared to the data from Ensemble in Fig. 3.5. The comparison of the plots shows good agreement between the fabricated filter and the simulated results. The slight shift in the frequencies is due to the difference in the dimensions of the fabricated filter and the simulated one. The accuracy of the fabricated dimensions are ±5% compared with the simulated dimensions.

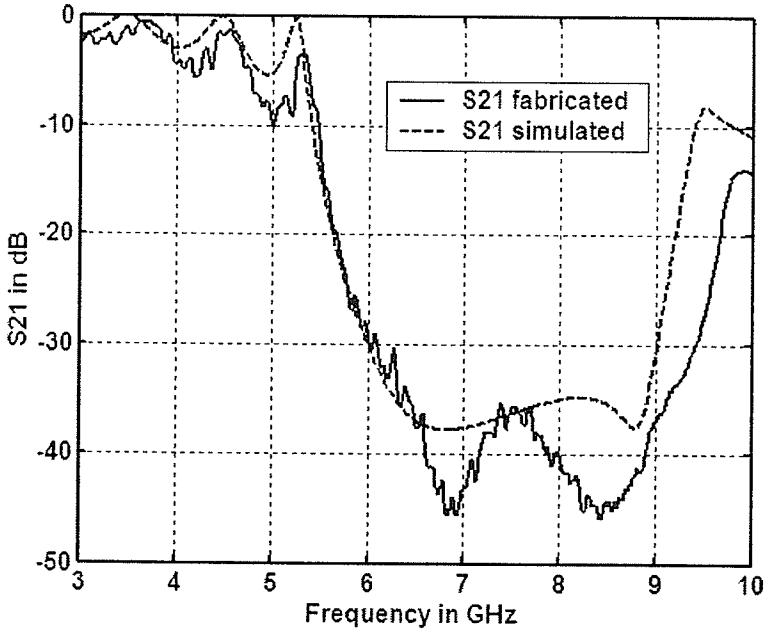

Fig. 3.5 S_{21} comparison of the fabricated and simulated filters with dimensions: L=102 mm, w=4 mm,r=3.2 h=1.59 mm, a=13 mm, d=11.6 mm

3.2 Wideband PBG Filter

The bandwidth of the filters shown so far are restricted to the dimensions of the holes. Since, there is a certain limit on the size of the holes that can be placed in the ground,

other configurations must be used to create filters with wider stopbands. This can be achieved by using one column of hole with more than one period creating multiple stopbands. If the stopbands are close to one another, a wide stopband or a narrowband filter with superior performance can be created. The geometry of such a structure is shown in Fig. 3.6.

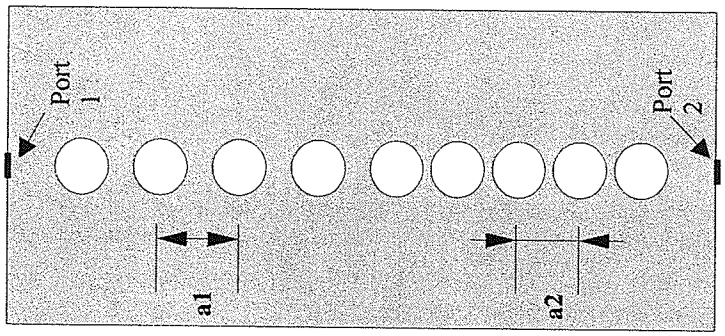

Fig. 3.6 Ground plane view of the wideband filter

Using Ansoft Ensemble, few different wideband filters were simulated. For the first wideband filter simulated a1 is 18 mm, and a2 is 13 mm corresponding to stopbands at 5.32 and 7.37 GHz. The S parameters for this filter are shown in Fig. 3.7.

It should be noted that the S_{12} and the S_{21} shown in Fig. 3.7 are identical and therefore only one of the curves is shown. For the filter in Fig. 3.6, the holes have a radius of 5.5 mm and a total of 9 holes is placed underneath the transmission line. Looking at Fig. 3.7, it can be seen, the filter has a wide stopband. Whether port 1 or port 2 is used as the feed, the filter will stop the transmission of EM waves between 3.55 and 9.3 GHz. In addition, due to the overlap of the stopbands between 5 to 7 GHz, S_{21} level of below -30 dB has been achieved.

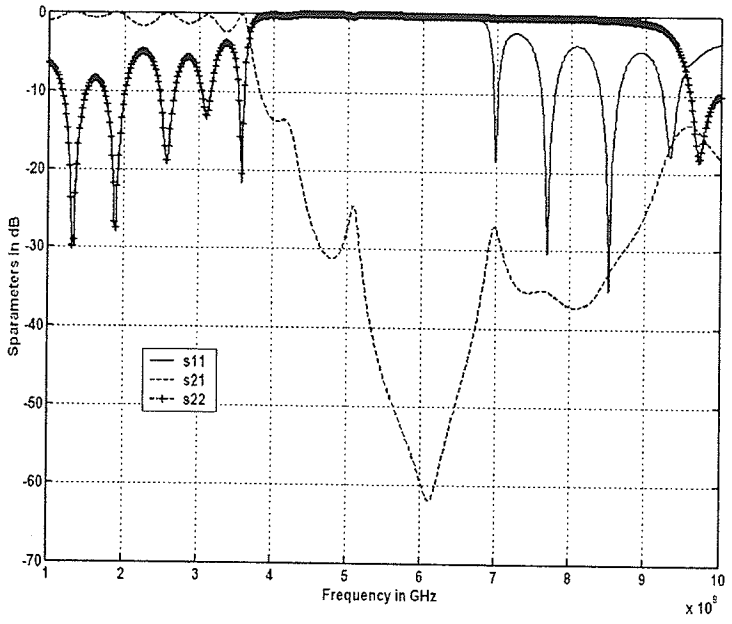

Fig. 3.7 S parameters of the simulated wideband filter

The above filter was also fabricated but the plots are not shown here. The S parameters were in good agreement with the simulated results.

Another combination simulated had period a_1 = 10.5 mm and a_2 = 6.5 mm. For this filter a really wide stopband from 7 to 17 GHz was obtained. However, at higher frequencies the circular holes in the ground start resonating and this leads to radiation from the structure. This can also be seen from the S parameters since the reflection from port 1 is low and at the same time there is no power transmitted to port 2.

3.3 Effective Permittivity

An important parameter to consider in the study of PBG filters is the phase of the transmission coefficient (S_{21}). Based on the transmission line equations, a forward traveling voltage on a line is given by [11] :

$$V_i^+ = V_o^+ \, e^{-j\frac{(2\pi f \sqrt{\epsilon_e} z)}{c}} \qquad (3.1)$$

where f and z are the frequency and the distance along the line length. The phase is determined by the frequency of operation, the distance along the length of the line, and ε_e which, is the effective dielectric constant for a particular structure. For comparison, the phase of S_{21} for the fabricated filter in Fig. 3.5 and the phase of S_{21} for the same structure with the holes in the ground covered with copper tape (i.e. To cancel the filter effect) are plotted in Fig. 3.8. Since we are interested in the passband of the filter, only the phase change between 30 kHz and 6 GHz is shown in Fig. 3.8.

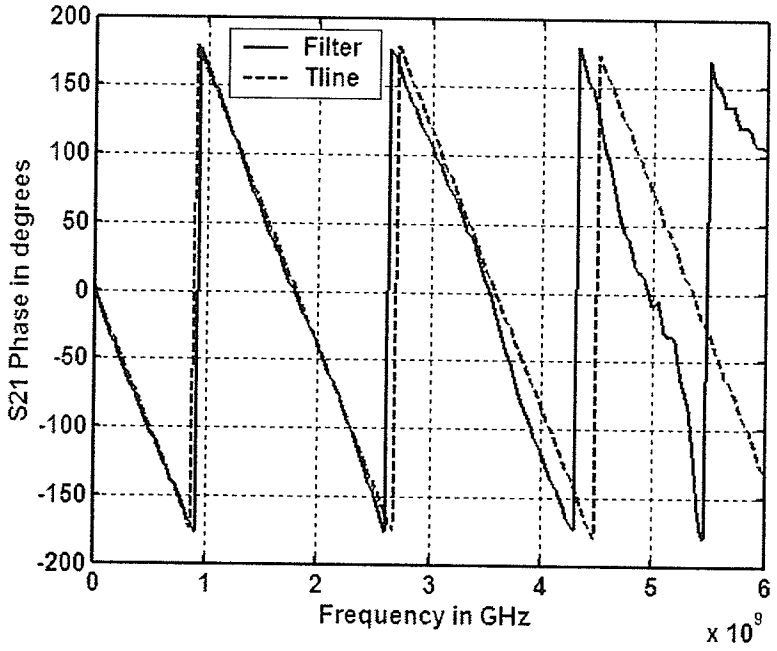

Fig. 3.8 Measured S_{21} phase of the fabricated filter and the transmission line vs. frequency

From the S_{21} phase plots of the transmission line, the phase change along the line is as expected from equation 3.1. However, for the filter this change in phase as a function of

frequency happens at a faster rate specifically between 4.3 and 5.5 GHz. Since everything else is identical for both cases, the faster rate of change in phase can only be due to the change of the effective epsilon in equation 3.1. The ratio of the phase change of the two structures for a particular frequency range would provide us with the effective epsilon ratios. These ratios are given in table 3.1 for different frequency ranges. In addition, the simulated phase ratios are also given in table 3.2 for comparison with the measured results.

Table 3.1. Filter and Transmission line Effective permittivity ratios obtained from the measured S_{21} phase

f_1 (GHz)	f_2 (GHz)	Δf	$\Delta\phi_{tline}$	$\Delta\phi_{filter}$	$\varepsilon_{filter}/\varepsilon_{tline}$
2.7	4.29	1.59	321.7	337.93	1.1
4.5	5.46	0.96	196.57	309.11	2.47

Table 3.2. Filter and Transmission line Effective permittivity ratios obtained from the simulated S_{21} phase

f_1 (GHz)	f_2 (GHz)	Δf	$\Delta\phi_{tline}$	$\Delta\phi_{filter}$	$\varepsilon_{filter}/\varepsilon_{tline}$
2.7	4.29	1.59	318.9	329.76	1.07
4.5	5.46	0.96	197	309.12	2.46

As it can be seen, the measured and simulated results are in good agreement. It is also observed that between 4.5 and 5.46 GHz, the filter has an effective epsilon value 2.46 times higher than the transmission line. This means that the characteristic impedance of the filter will be $(1/\sqrt{2.46})$ smaller than the characteristic impedance of the transmission line. In order to calculate the actual epsilon values for the filter, a Matlab program was written in which the epsilon values are calculated from the reflection coefficient (S_{11}) parameter obtained from Ensemble. Knowing the reflection coefficient, and the

impedance of ports 1 and 2 (Z_{port}) of the structures, one can find the input impedance from the following equation [11]:

$$Z_{input} = Z_{port} \frac{(1+S_{11})}{(1-S_{11})} \qquad (3.2)$$

In addition, the input impedance can be found from:

$$Z_{input} = Z_o \frac{(Z_L + Z_o \tanh \gamma l)}{(Z_o + Z_L \tanh \gamma l)} \qquad (3.3)$$

where Z_L is the load impedance, γ is the propagation constant, and Z_o is the characteristic impedance of the line. Note that In equation 3.3 both the characteristic impedance and the propagation constant are functions of the effective epsilon.

Therefore, by equating equations 3.2 & 3.3 one can solve for the effective epsilon. This is done by using an iterative process in which the epsilon values are increased by small increments and the input impedance in equation 3.3 is calculated for each increment and compared with equation 3.2. Using this procedure, the characteristic impedance and the effective permittivity values were computed for several frequencies for both the filter and transmission line and are shown in tables 3.3 and 3.4 respectively.

Table 3.3. Characteristic impedance and permittivity values of the filter obtained from the Matlab program

Frequency (GHz)	ε_{filter}	Z_o
3.476	**2.54**	**48.96**
***4.00**	**2.92 + i0.48**	**45.2 – j3.7**
4.47	**2.64 + j0.1**	**48 – j0.9**
5.24	**3.84 + j0.02**	**40 – j0.1**

The frequencies in tables 3.3 except at 4 GHz, are the frequencies where there is minimum return loss (S_{11}). This can be seen in Fig. 3.5 where the S_{21} is almost equal to zero. At 4 GHz however, there is some reflection and the effect of the reflection can be seen in the effective epsilon value. The effective epsilon in table 3.3 at 4 GHz has a large imaginary part which is due to the reflection at the input.

Table 3.4. Characteristic impedance and permittivity values of the transmission line obtained from the Matlab program

Frequency (GHz)	ε_{tline}	Z_o
3.476	**2.44+ j0.02**	**50 – j0.2**
***4.00**	**2.4000**	**50.37**
4.47	**2.40 + j0.02**	**50.37 – j0.2**
5.24	**2.38+ j0.02**	**50.58 – j0.21**

In both tables the same frequencies are used for comparison of the transmission line with the filter. As it can be seen, the values of the effective epsilon of the filter in table 3.3 are higher for all the frequencies particularly at 5.24 GHz which, is right before the stopband of the filter. The same observations were made in regards to the effective epsilon values of the wideband filter.

It should be noted that due to the roundoff process in the iteration technique used in the program, there are errors associated with the effective permittivity values listed in tables 3.3 and 3.4. Overall however, an increase in the permittivity values of the filter is observed.

Another method of measurement of the effective epsilon investigated involved the use of a probe to sample the S_{21} phase along the transmission line and the filter. The probe was used to take samples as it moved at small increments along the transmission line for different frequencies. Looking at equation 3.1, the phase of the forward traveling wave changes as a function of position (i.e. z) for a fixed frequency. Therefore, as the wave travels along the transmission line it will go through a 360 degree phase shift corresponding to one wavelength. Once the wavelength is obtained, the effective epsilon can be calculated from:

$$\epsilon_e = \left(\frac{C}{(\lambda f)}\right)^2 \qquad (3.4)$$

where, C is the speed of light and f is the frequency of operation. Using this procedure the effective epsilon values for the fabricated narrowband and wideband filters were calculated for a few different frequencies. However, for the narrowband filter, due to its short length and multiple reflections from the holes in the ground, it was not possible to obtain clear samples of the wavelengths. The samples taken from the wideband filter were more clear. The effective permittivity values for both the filter and transmission line (i.e. filter with the ground plane holes covered with copper tape) are shown in table 3.5. Looking at the data in table 3.5, the effective epsilon value for the filter at 3.7 GHz is 2.98 while for the transmission line a value of 2.63 is obtained. Therefore, the simulation results are now confirmed with experimental measurement. It should be noted that the data shown in table 3.5 are approximate. There were many different sources of error in the experiments some of which include the presence of noise from different sources during the sampling process, the position of the probe with respect to the filter,

and discrepancies in the fabricated dimensions of the filter.

Overall however, the measured data shows an increase in the epsilon value of the filter right before the stopband of the filter at 3.7 GHz which, was confirmed by the software previously.

Table 3.5 Effective epsilon values obtained from sampling of the wavelength on the filter and transmission line

f (GHz)	ε_{tline}	ε_{filter}
3.00	2.70	2.60
3.20	2.55	2.44
3.50	2.55	2.39
*3.70	2.63	2.98

3.4 Conclusion

In this chapter microstrip transmission lines with ground plane perforations were studied. It was shown that by etching holes in the ground plane of a transmission line, different types of microstrip filters can be created. The holes etched in the ground had different geometry's and dimensions. The effects of hole dimensions and period on the performance of filters were studied in detail. It was shown that the filter stopband is determined by the hole period while the stopband bandwidth is determined by the hole size. In addition, by the use of PBG structures, with more than one period, a new wideband filter was designed. The designed filter showed very low isolation levels (S_{21} $\leq$-30 dB) due to the bandgap overlap. In order to verify the simulated data, one of the filters was fabricated and tested and the measured data showed good agreement with the

simulated results.

Finally, it was shown that by etching of holes in the ground plane of transmission lines, the effective permittivity of the structures is increased. The effective permittivities were calculated for different filters using a Matlab code. For the wideband filter, the effective permittivity was calculated by measuring the wavelength on the surface of the filter. The wavelength was measured using a probe that moved on the surface of the filter. The measured permittivity of the filter showed an increase in value compared with that of a simple transmission line.

Chapter 4

Microstrip Patch Antennas with Ground Plane Perforations

In this chapter, the properties of microstrip patch antennas on perforated ground planes are studied in detail. Different perforation types such as holes and slots are placed in the ground planes of wideband and narrowband patch antennas. For each case, the effects of the perforations on the resonant frequency, gain, and the bandwidth of the antennas are investigated.

4.1 Narrowband Patch Antennas with Ground Plane Perforations

In this section, different ground plane perforations such as a single hole, multiple holes and slots in the ground plane of different narrowband patch antennas are investigated.

4.1.1 Narrowband patch antenna with a single hole in the ground

In the previous chapter it was found that by placing holes in the ground plane of a microstrip transmission line, an increase in the effective epsilon can be achieved. As a next step, the holes were placed in the ground plane of microstrip patch antennas to see the effects on the resonant frequency and effective epsilon of the patch. The first case that was simulated involved an antenna with the geometry shown in Fig. 4.1. The antenna contains a square hole of dimensions (d × d) in the ground plane. A circular hole underneath the patch was also simulated. However, this geometry is not shown here. The patch antenna for all the cases has a length of 15 mm and width of 20 mm. The

substrate has a relative permittivity of 3.2 and a thickness of 0.79 mm (1/32″).

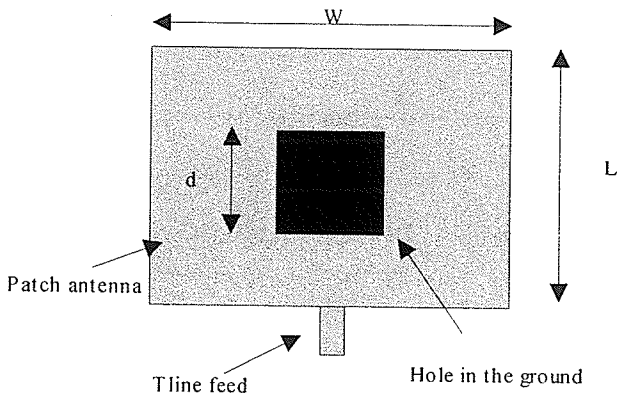

Fig. 4.1 Geometry of a patch antenna with a hole in the ground plane
L = 15 mm W = 20 mm ε_r = 3.2 h = 0.79 mm

For this antenna, the dimensions of the hole underneath the patch were changed and the effects on the resonant frequency, – 10 dB bandwidth and, the gain were recorded. Plots of the resonant frequency, bandwidth, and the gain vs. the holes area are shown in Fig. 4.2a-c for both a rectangular hole and circular hole. As it can be seen from Fig. 4.2a, the resonant frequency of the patch drops as the area of the holes in the ground plane is increased. The rate of change of frequency is different for the two hole structures, due to different effective areas. Looking at equation 4.1, the resonant frequency of the patch is defined in terms of the antenna length and the permittivity of dielectric material.

$$f_r = \frac{C}{(2L\sqrt{\epsilon_e})} \qquad (4.1)$$

Therefore, it is obvious that for a fixed length, a drop in the resonance is due to an increase in the effective epsilon of the structure.

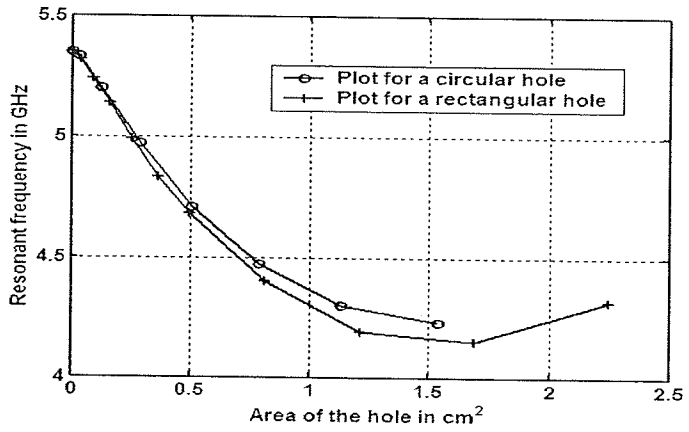

(a)

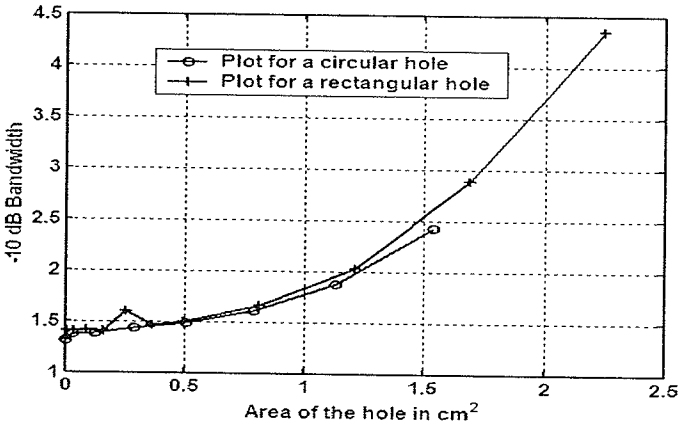

(b)

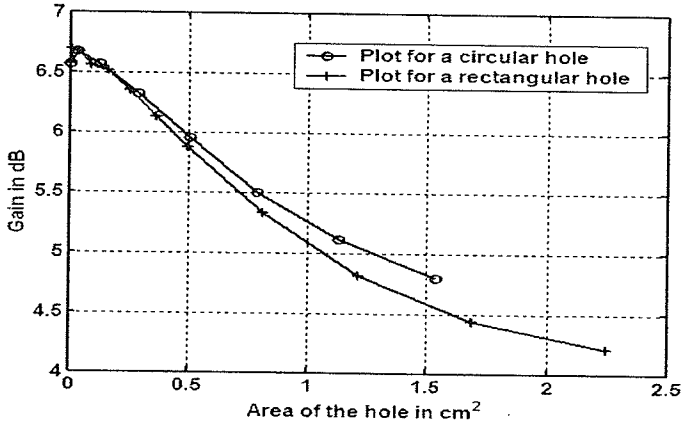

(c)

Fig. 4.2 (a) Resonant frequency vs. hole area (b) -10 dB bandwidth vs. hole area (c) Gain vs. hole area for the patch shown in Fig. 4.1

In addition to the shift in the resonance, it was also observed that the -10 dB bandwidth of the patch increases as the hole area in the ground is increased, Fig. 2-b. However, as one might expect there is a significant drop in the gain for larger perforations, which is due to the increase in back radiation levels.

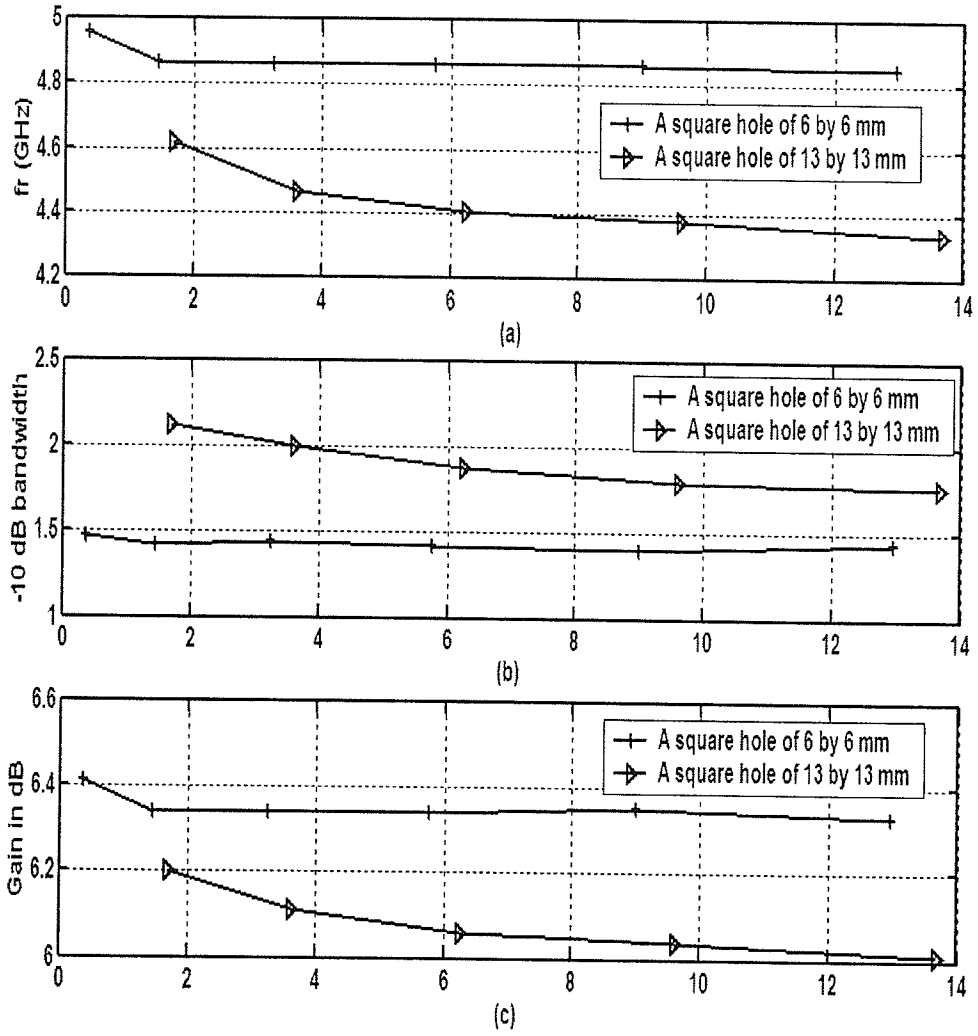

Fig. 4.3 (a) Resonant frequency vs. cavity area in cm² (b) -10 dB bandwidth vs. cavity area in cm² (c) Gain in dB vs. cavity area in cm²

In order to prevent the back radiation, a cavity was placed underneath the antenna. By placing the cavity under the antenna, the antenna gain increased as expected. However, the bandwidth of the antenna reduced thereby canceling the effects of the hole in the ground plane. The plots of resonant frequency, bandwidth and gain for two different square hole dimensions (6 by 6 mm and 13 by 13 mm) as a function of the cavity area are shown in Fig. 4.3a-c. The cavity height for all the cases is fixed at 3.175 mm.

4.1.2 Narrowband patch antenna with multiple holes in the ground:

For this section, the narrowband patch antenna with a photonic bandgap ground plane (PBG ground) [4] was simulated in Ensemble. According to the authors in [4], the photonic bandgap ground plane has the effect of suppressing the higher unwanted modes. The geometry of this square patch with the dimensions is shown in Fig. 4.4.

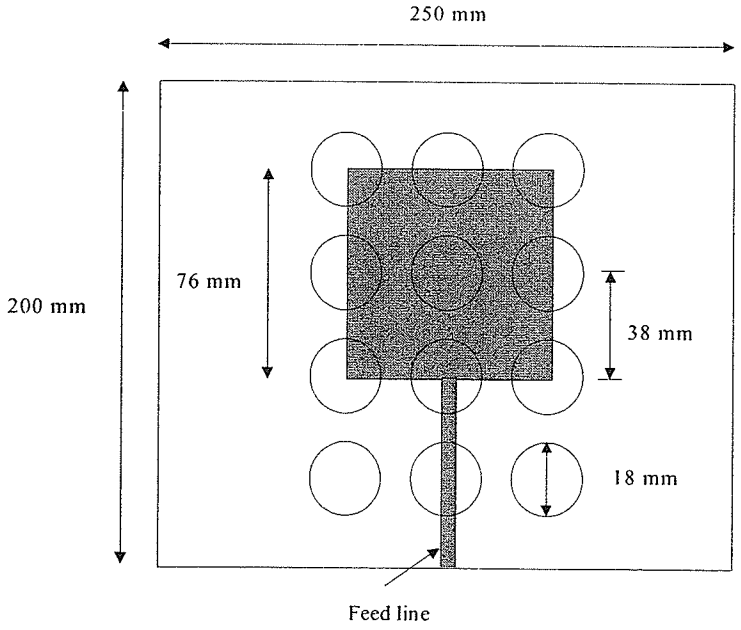

Fig. 4.4 Narrowband PBG patch antenna

The patch has a length and width of 76 mm. The substrate material for this antenna has a dielectric constant of 4.8 and a thickness of 1.6 mm. The width of the transmission line feed is 2.8 mm, corresponding to a 50 Ω line, and its length is 78 mm. The holes in the ground have a center to center spacing of 38 mm which, correspond to a center stopband frequency of 1.8 GHz [4]. The holes here have the same function as the holes placed underneath the transmission line in the previous chapter. The reflection coefficient of this antenna with and without the PBG are shown in Fig 4.5a and b, respectively.

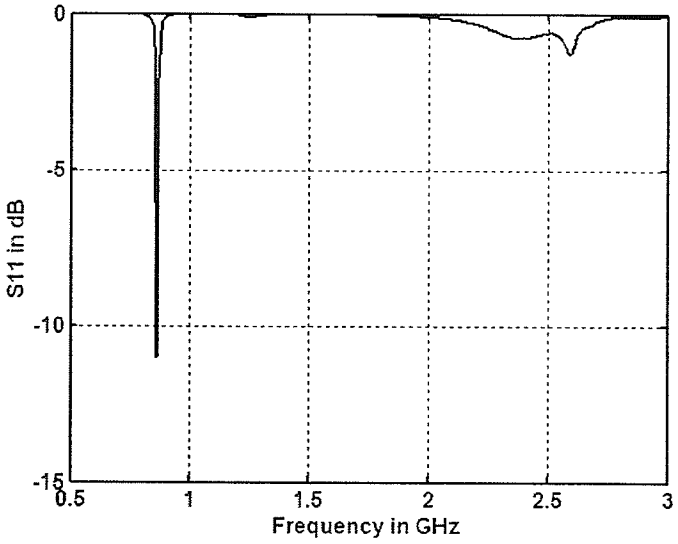

Fig. 4.5 (a) The reflection coefficient of the PBG antenna

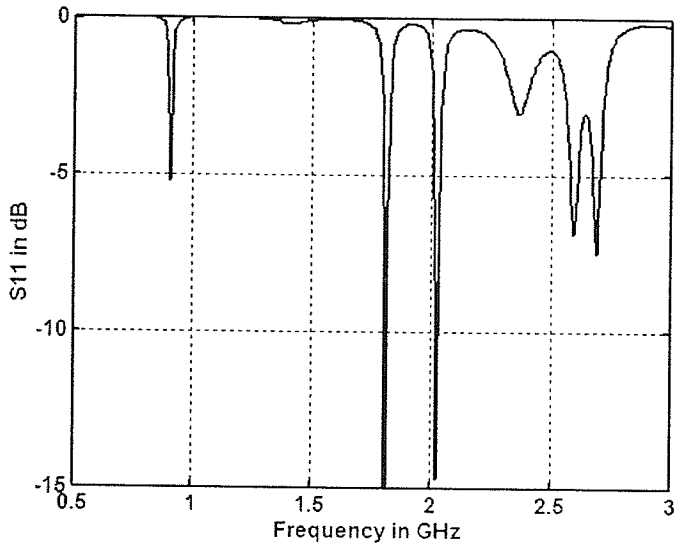

Fig. 4.5 (b) The reflection coefficient of the reference antenna

As it can be seen from the S_{11} plot of the reference patch, the dominant mode occurs around 0.9 GHz, while the higher order modes around 1.8 and 2.1 GHz are excited as well. The reflection coefficient of the patch with the PBG ground plane shows disappearance of the higher order modes around 1.8 GHz which is the stop band of the PBG. These modes are still present however, their excitation is prevented by a combination of different factors such as the geometry and the position of the PBG structure as well as the finite ground plane size. In order to see the sensitivity of this structure, the number of holes in the ground plane were changed and the S_{11} for the two different cases are shown in Fig. 4.6. For the first case, the hole underneath the transmission line was removed but the remaining holes were present. This configuration removed the higher order modes but other resonances occurring close to the dominant mode.

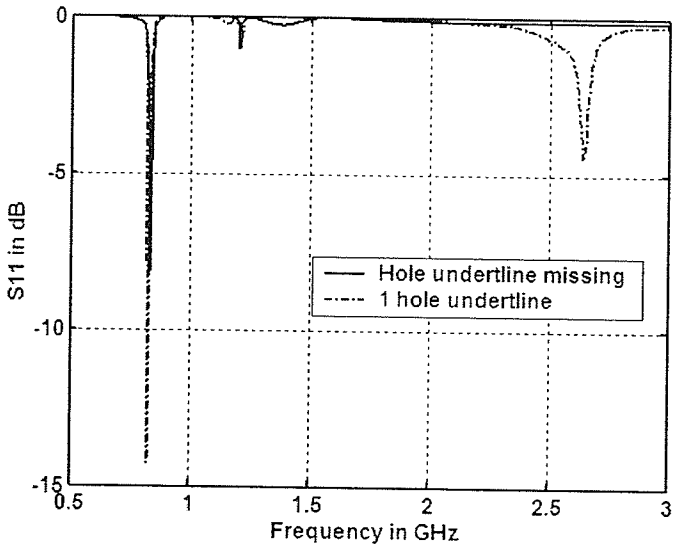

Fig.4.6 The reflection coefficient for different PBG patch antenna configurations

The second graph shows the S parameters for the patch with a single hole underneath the transmission line feed and the adjacent two holes removed (Note that the holes underneath the patch are still present). Once again the excitation of higher order modes can be seen in the S_{11} plot. Finally, to investigate the effect of the ground plane size on the results, an infinite ground plane was used instead of a finite ground. The S_{11} of the patch with infinite ground is shown in Fig. 4.7. As it can be seen, by use of an infinite ground plane, a second mode close to the dominant mode is excited.

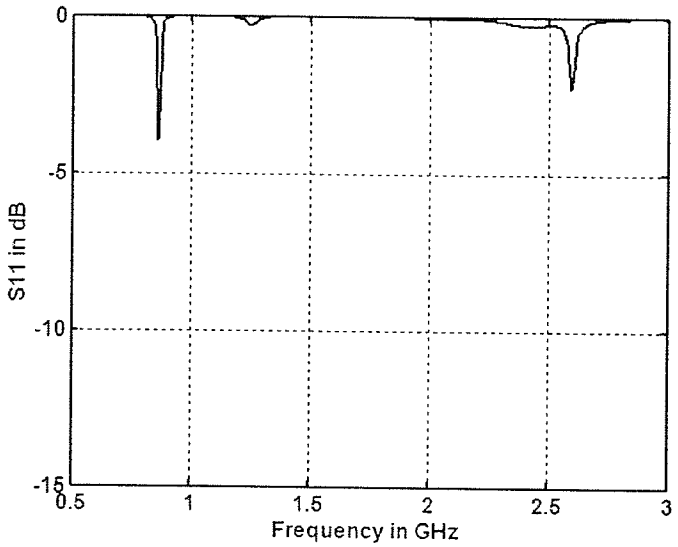

Fig. 4.7 Reflection coefficient of the PBG antenna with infinite ground plane

4.1.3 Narrowband patch antenna with slots in the ground:

The geometry of this antenna with the slots in the ground plane is shown in Fig. 4.8. This patch has a length of 15 mm and a width of 20 mm. The dielectric material used is the same as before with a permittivity of 3.2 and a thickness of 1/32". For this antenna, a probe feed is used instead of a transmission line feed for all the simulations.

To see the effects of the slots in the ground plane, slots with different dimensions were placed in different positions in the ground. For all the cases two slots were placed in the ground to have a symmetric condition. Different parameters such as the the width of the slots W, the distance from the center of the patch to the edge of the slots d and, the length of the slots L were changed and the results on the resonant frequency were recorded for each case. The reflection coefficients for a few different cases are shown in Fig 4.9.

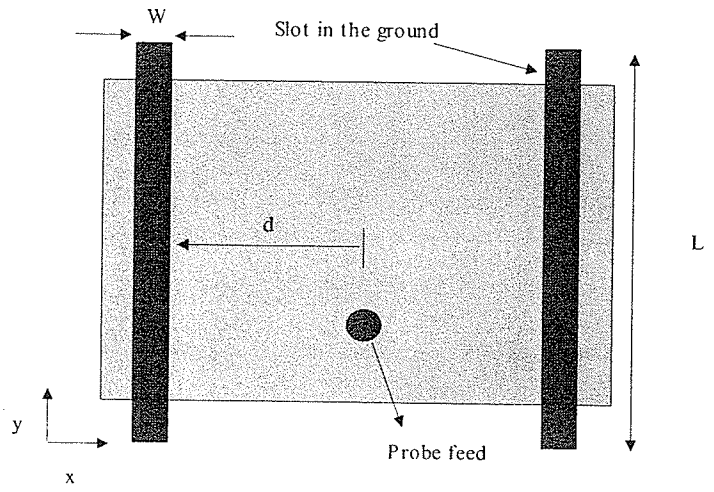

Fig. 4.8 Geometry of the patch antenna with slots in the ground plane

The dominant mode for the reference patch with no slots in the ground occurs at 5.3 GHz.

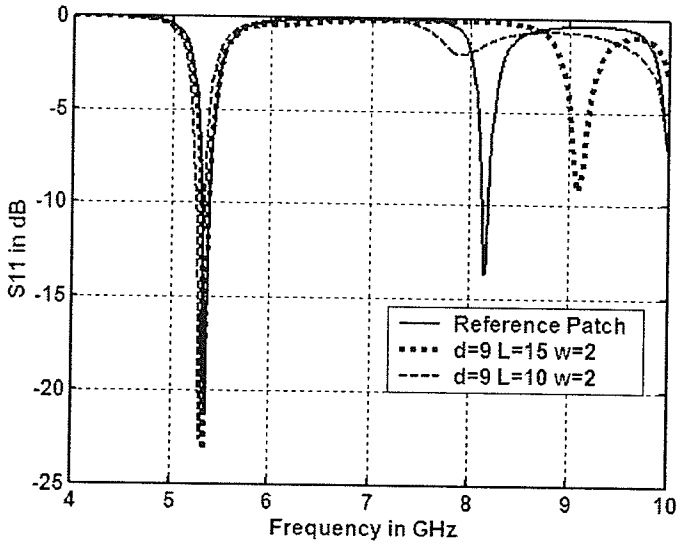

Fig. 4.9 The reflection coefficient for the reference patch and the patch with slots in the ground along the y direction (Dimensions of the slots are in mm)

For the patch with slots in the ground, there is no shift in the frequency of the dominant mode at 5.3 GHz. However, there is a shift in the resonance of the next higher order mode at 8.2 GHz. For the antenna with the slot length of 15 mm, a shift of 1 GHz in the resonance of the unwanted mode is observed. The shift in frequency of the higher order modes can be a useful tool in cases where the frequency of the dominant mode is close to the unwanted higher order modes. As one might expect, there is a drop in the gain of the antenna due to the back radiation from the slots. The use of the cavity could solve the back radiation problems. However, this leads to other resonances created by the cavity.

In addition to the slots along the y direction, the slots were also placed in the x direction (placed along the width of the patch), but this created a shift in the resonance of the dominant mode as well as excitation of other modes close to the dominant mode. An example of this is shown in Fig. 4.10. Note that here *d* is the distance from the center of the patch to the edge of the slot, located along the x direction.

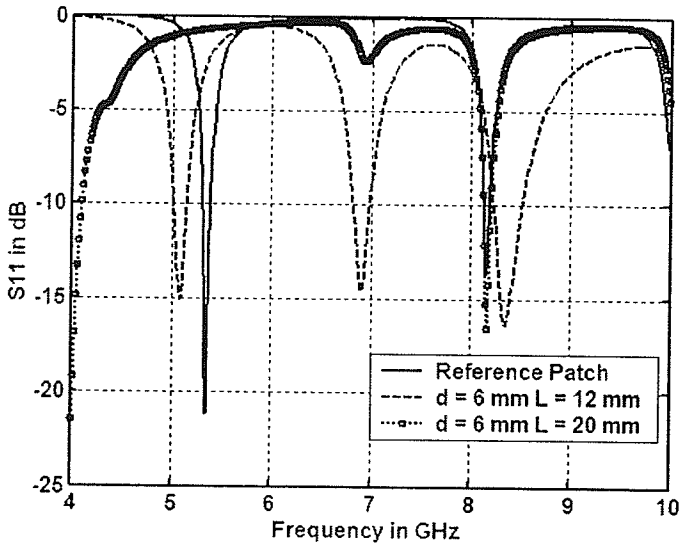

Fig. 4.10 The reflection coefficient for reference patch and the patch with slots in the ground along the x direction (Dimensions of the slots are in mm)

4.2 Wideband U-Slot Patch Antenna with Ground Plane Perforations

In order to see the results of ground plane perforations on wide band microstrip antennas, the U-slot antenna that was designed by R. Bhalla and L. Shafai [15] was simulated with slots in the ground plane of the patch. The geometry of the reference antenna and the antenna with slots in the ground are shown in Fig. 4.11 and 4.12 respectively.

For this antenna, the slots were placed along the width of the patch as shown in Fig. 4.12. Once again the parameters of the slots were changed and the effect on the S_{11} was recorded. The S_{11} of the reference antenna along with the antenna with ground slots are shown in Fig. 4.13. The reference antenna has a -10 dB bandwidth of 30%, while the antenna with the slots of parameters $d = 12$ mm, $L = 26$ mm and $W = 9$ mm in the ground, has an increased bandwidth of 37%.

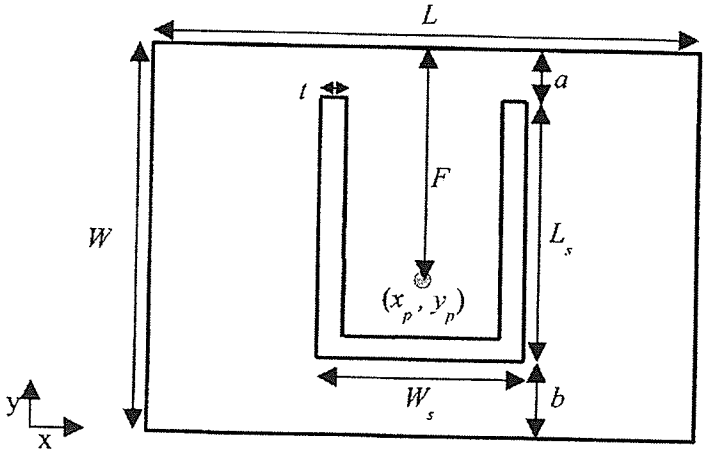

Fig. 4.11 Geometry of the reference Uslot patch antenna, L = 35.5, W = 26, L_s = 19.5, W_s = 12, t = 2.1, F = 15, h = 5.0, a = 4.2, b = 2.3. All dimensions in mm [15]

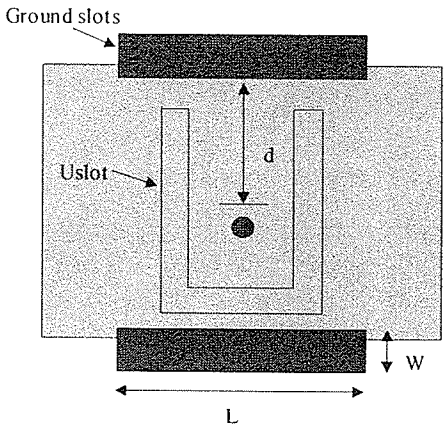

Fig. 4.12 Geometry of the Uslot patch antenna with slots in the ground plane

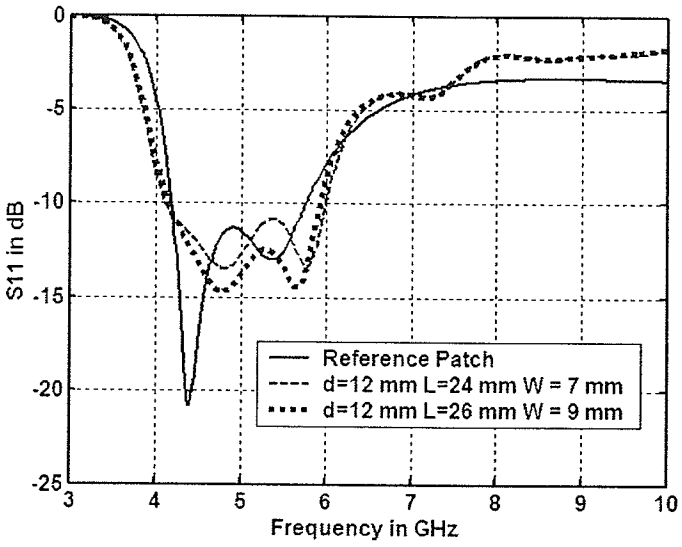

Fig. 4.13 The reflection coefficient of the Uslot with and without the ground plane slots

To reduce the back radiation levels, a cavity was placed underneath the antenna. However, this reduced the bandwidth of the patch significantly. The S_{11} of the Uslot with ground slots of dimensions d = 12 mm, L = 26 mm and W = 9 mm, with a cavity

underneath the patch is shown in Fig. 4.14. Note that the height of the cavity is fixed at 2 mm.

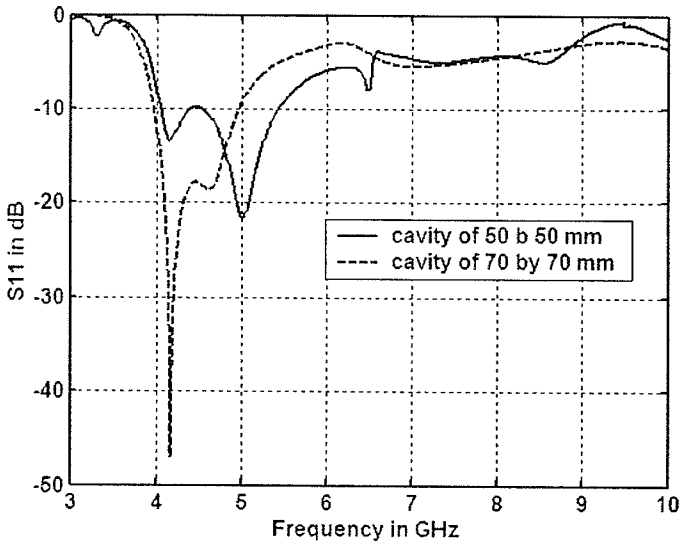

Fig. 4.14 The reflection coefficient of the cavity backed Uslot with slots of dimensions of d = 12 mm, L = 26 mm and W = 9 mm in the ground plane

In addition to slots in the ground plane, a square hole was also placed underneath the patch to see the effects on the resonance of the patch. In order to excite the patch using a probe, a cavity had to be placed below the square hole. Since the probe passes through the cavity, the structure of the cavity is changed by the parameters of the probe. The presence of the cavity caused a reduction in the bandwidth of the antenna and created a third resonance close to the first two resonances of the patch.

4.3 Conclusion

This chapter was a study of microstrip patch antennas with ground plane perforations. Different types of perforations such as a single hole, multiple holes and slots were placed in the ground plane of patch antennas. The perforations were used in the design of both narrowband and wideband patch antennas. For the narrowband patch antennas, the use of a single hole in the ground plane showed a decrease in the resonant frequency and an increase in -10 dB bandwidth of the patch. The decrease in the resonant frequency can be explained by an increase in the permittivity of the structure. The use of perforations in the ground has the effect of decreasing the overall gain of the patch due to the increase in the back radiation. The use of a cavity to reduce the back radiation canceled the effects of the hole in the ground plane.

In addition to a single hole, multiple holes were also used in the design of narrowband patch antennas. It was found that by the use of multiple holes, the excitation of higher order modes can be prevented. This was also accomplished by the use of slots in the ground plane of a narrowband patch antenna. A shift in the resonance of higher order modes was achieved by placing slots in the ground plane, along the length of the patch.

The slots in the ground plane were also used in a wideband U-slot patch antenna to increase its -10 dB bandwidth. Once again, a reduction in the gain was observed due to the back radiation from the slots in the ground plane.

Chapter 5

High Impedance PBG Structures

In this chapter, the properties of PBG structures consisting of metal patches with shorting vias on different substrate materials are investigated. For each PBG structure, Ansoft Ensemble is used to measure the radar cross section (RCS) of the TM waves vs. frequency, due to a wave incident on the structure. Once the bandgap of the TM modes for the PBG structures are found, the structures are then used in the design of microstrip patch antennas operating at the bandgap of the frequency. The effects of the PBG on the resonant frequency, gain and half power beamwidth of the antennas are investigated for each substrate material.

5.1 High Impedance Photonic Bandgap Structures

The geometry of a high impedance PBG is shown in Fig. 5.1. This structure consists of metal patches with shorting vias connecting the patches to the ground plane of the structure. If the dimensions of the geometry in figure 5.1 are small compared to the wavelength, the impedance of the structure can be modeled by an equivalent parallel resonant LC circuit [10]. The inductance of this circuit is due to the vias while the capacitance is due to the gap between the adjacent patches. As mentioned in chapter 2, the surface impedance of this structure is characterized by [10]:

$$Z = \frac{(j\omega L)}{(1-\omega^2 LC)} \qquad (5.1)$$

The resonant frequency of the LC circuit is given by:

$$\omega_o = \frac{1}{\sqrt{(LC)}} \qquad (5.2)$$

At the resonant frequency the surface impedance becomes very high and this is associated with the band gap of the structure [10].

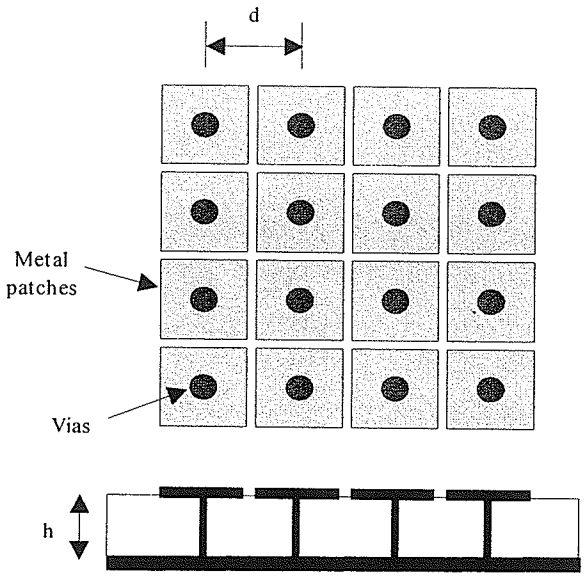

Fig. 5.1 Geometry of the PBG structure

Since the resonant frequency is inversely proportional to the inductance and the capacitance of the PBG, it can be controlled by the dimensions and spacing of the metal patches as well as the length and diameter of the vias. In order to find the band gap of the geometry in figure 5.1, Ansoft Ensemble was used to measure the RCS (i.e. reflection) vs. frequency, due to an incident wave on the structure. Since the structure behaves as an open circuit at its resonant frequency, one would expect reflection of the incident wave at the resonance. For the PBG design, we are interested in the stopband of the TM surface

wave which, propagates along the dielectric surface. The TM surface waves have no cutoff frequency and decay exponentially away from the dielectric air interface [11]. The presence of these surface waves is specially evident in structures with a high dielectric constant and large thickness [1].

An example of the radar cross section of a TM mode for two different PBG structures, on a substrate with a relative permittivity of 3.2 and a substrate thickness of 1.59 mm, is shown in Fig. 5.2. The first case uses metal patches of dimensions 6 mm by 6 mm and the second uses patches of dimension 8 mm by 8 mm. For both cases, the spacing between the edges of the adjacent patches are 0.2 mm and the vias used have a radius of 0.6 mm. The radar cross sections (RCS) shown below are for the TM modes looking in the same direction as the incident wave, i.e. the back scattering cross section.

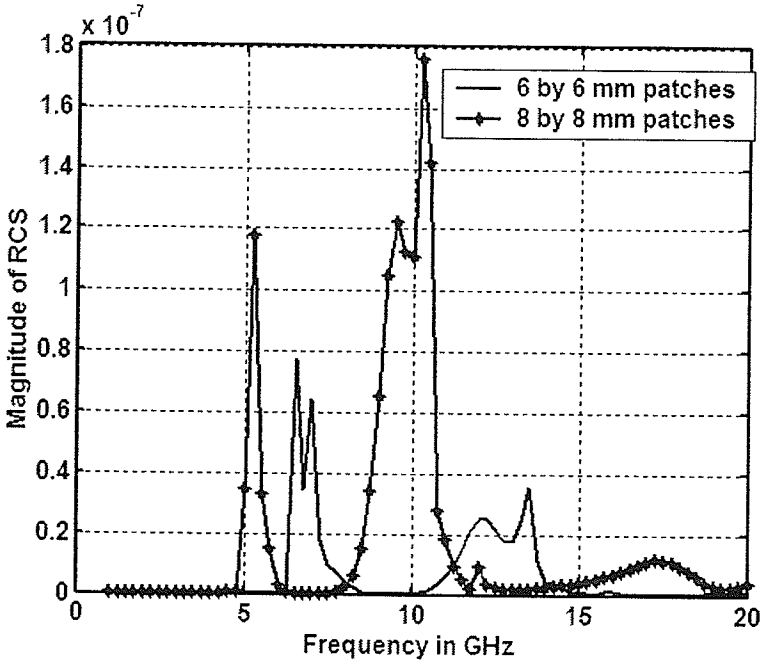

Fig. 5.2 Magnitude of RCS vs. frequency for the two different metal patch sizes on a substrate with ε_r = 3.2 and h = 1.59 mmm (wave incident horizontally)

As it can be seen from Fig. 5.2, the RCS for the design with dimensions of 6 mm by 6 mm has peak reflections between 6.25 to 8.5 GHz and another between 10.25 to 14.75 GHz. As expected, the structure with metal patches of size 8 mm by 8 mm has peak reflections occurring at lower frequencies due to the increase in capacitance of the structure. For the 8 mm by 8 mm patch, the first reflection peak occurs between 4.75 to 6.25 GHz and second between 8 to 11.75 GHz. The same procedure can be applied to all PBG structure on other dielectric materials to find the reflection of the TM waves as a function of frequency.

5.2 High Impedance Structures and their Applications in Microstrip Patch Antennas

In order to better understand the behavior of PBG structures, different patch antennas with various PBG structures on different dielectric materials were simulated in Ensemble. The dielectric materials used had ε_r = 9.8, 3.2, 2.5, and 1. For each case the effects on the resonant frequency, gain, and half power beamwidth of the antennas were studied. It should be noted that, for all simulation results to be presented in this chapter, the loss tangent used for the substrates were set to **(0.0001)** and therefore all the gain values are for low loss substrates. Due to problems with the simulation software, the substrate material with relative permittivity of 9.8 is covered in the last section of this chapter.

5.2.1 Patch Antennas on ε_r = 3.2 PBG Substrate

In this section, the properties of PBG patch antennas operating at two different

frequencies are investigated. Since, the RCS of the PBG in Fig. 5.2, has a peak reflection between 4.75 and 6.25 GHz, the first patch simulated was designed to operate at 5.6 GHz. The patch is probe fed and has dimensions L = 14 mm, W = 20 mm, and h = 1.59 mm (1/16″). The ground plane is finite for this patch and has dimensions 80 mm by 80 mm (1.5λ). The simulated radiation patterns in the E and H planes ($\phi = 90$ and $\phi = 0$) are shown in figure 5.3. As it can be seen from the gain plots, the co-polar E plane pattern is wider than the co-polar H-plane pattern and has a dip at $\theta = 0$ which, is due to the size of the finite ground plane. There is also a large amount of back radiation caused by the diffraction from the finite ground plane edge, which will be shown later. The back radiation levels reach as high as -5 dB at $\theta = 100$ degrees.

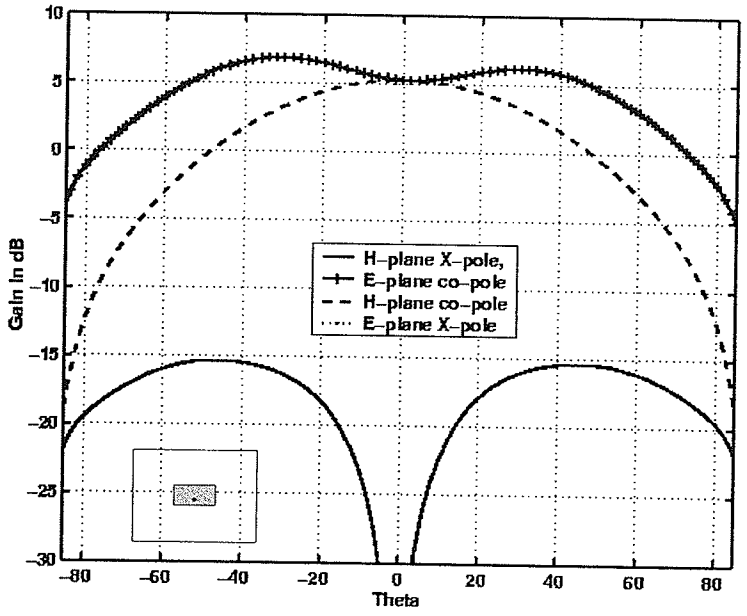

Fig. 5.3 E and H plane patterns of the reference patch with L = 14 mm, W = 20 mm, h = 1.59 mm, $\varepsilon_r = 3.2$, tan $\delta = 0.0001$, at 5.6 GHz

The second patch antenna simulated has a length of 7 mm corresponding to a resonance at 10.95 GHz. The width of the patch is 12 mm and the ground plane size is 40 mm by 40 mm. The substrate height is the same as before at 1.59 mm. The radiation patterns for this patch are shown in Fig. 5.4. Once again, a dip in the E plane co-polar pattern at $\theta = 0$ is observed.

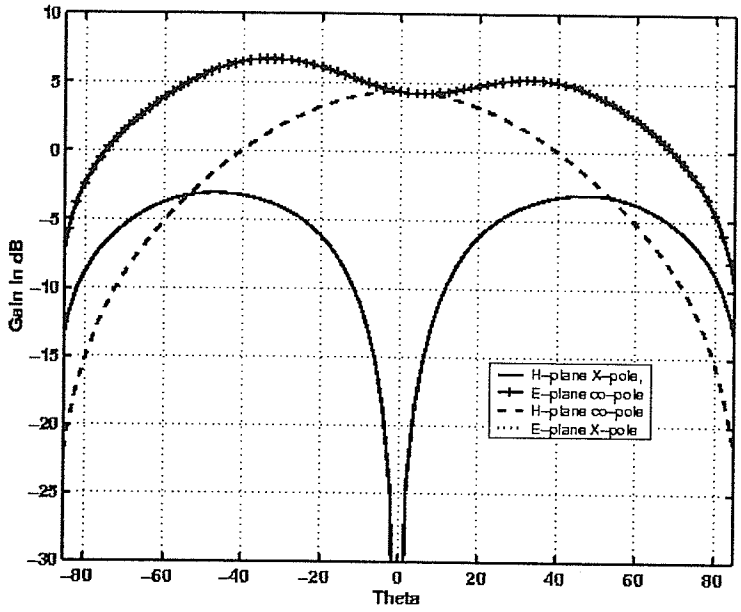

Fig. 5.4 E and H plane patterns of the reference patch with L = 7 mm, W = 12 mm, h = 1.59 mm, ε_r = 3.2, tan δ = 0.0001, at 10.95 GHz

Next, the patch antennas with PBG structures were simulated and the effect of the PBG on the resonant frequency, gain and half power beamdwidths were recorded. For each antenna the PBG structures were placed around the patch as shown in Fig. 5.5. As it can be seen from Fig. 5.5, only a single layer of metal patches was used around the microstrip antenna. This provided the highest gain compared with a multilayered structure. Use of

multiple layers around the patch causes a drop in the gain thereby canceling the effect of the PBG. In addition, there is a large increase in the cross-pole levels caused by the vertical currents in the vias.

The use of the PBG structure around the patch has the effect of shifting the resonant frequency of the patch, as well as reducing its -10 dB bandwidth. The change in the resonant frequency can be adjusted by moving the PBG structure away from the antenna and leaving a gap between the antenna and the shorted metal patches. However, the reduction of the bandwidth is a negative effect of the PBG.

Since the two patch antennas discussed so far have different resonant frequencies, the PBG structures used for each patch were different. For the antenna operating at 5.6 GHz, the PBG has metal patches of dimensions 8 mm by 8 mm and spacing of 0.2 mm with the RCS shown in Fig. 5.2.

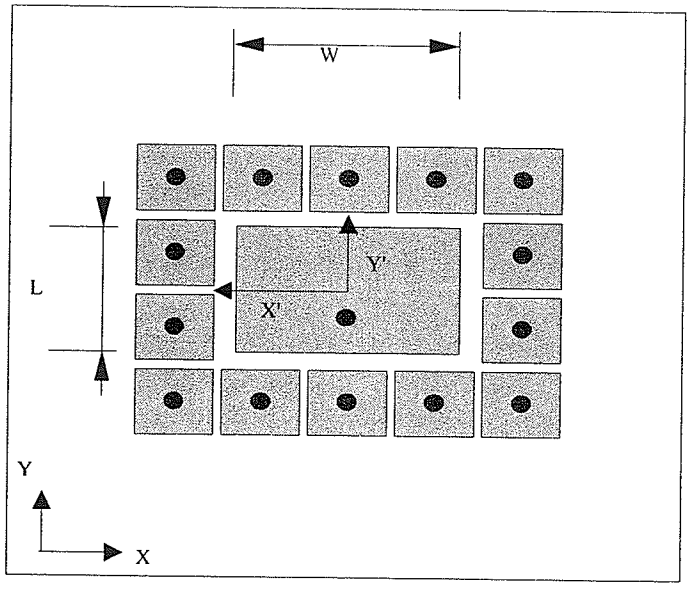

Fig. 5.5 Geometry of the patch antenna with PBG structure and finite ground plane

The use of the PBG around the patch caused the resonant frequency of the patch to be shifted to 5.78 GHz, compared to 5.6 GHz of the reference patch antenna. Its -10 dB bandwidth was also reduced significantly. The S parameters of this patch and the reference patch will be shown in the next chapter for comparison with fabricated antennas. The radiation patterns of this antenna are shown in Fig. 5.6. It can be seen that the gain of the patch has increased to 9.6 dBi from 5.3 dBi at $\theta = 0$ and the radiation pattern in the co-polar E-plane has improved significantly. Unlike the E-plane pattern of the reference patch shown in Fig 5.3, the E plane co-polar pattern is narrower than the H-plane co-polar pattern for the PBG patch antenna and the dip at $\theta = 0$ has disappeared.

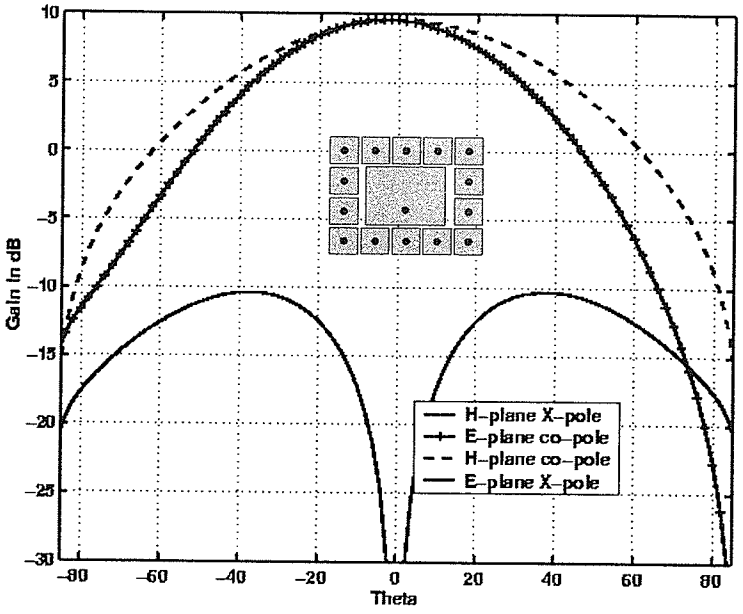

Fig. 5.6 E and H plane patterns of the PBG patch with L = 14 mm, W = 20 mm, ε_r = 3.2, tan δ = 0.0001, h = 1.59 mm, X′ = 12.4 mm , Y′ = 8.3 mm at 5.78 GHz

The slight increase in the H-plane cross-pole levels of the PBG antenna can be adjusted by moving the PBG structure away from the patch in the (x) direction without affecting the over all gain. As mentioned previously, this increase in the H-plane cross-pole level is due to the vertical currents that are generated in the vias. The vertical currents have a symmetric E_θ associated with them, which adds to the cross-polar patterns of the patch. By moving the PBG structure away in the y direction, the gain of the antenna drops and the resonant frequency shifts down as expected.

In addition, to the increase in the gain of the antenna in Fig. 5.5, the back radiation levels has dropped significantly to -14 dB compared with -5 dB at θ = 100 degrees. For comparison, the back radiations of both reference and PBG patch antenna are shown in Fig. 5.7 a and b, respectively. The E-plane cross-polar pattern is negligible and can not be seen in the back radiation plots due to it's value being less than -30 dBi. The resonant frequency, half power beamwidth, and the gain of the reference, Fig. 5.3, and PBG antennas, Fig. 5.5, are shown in Table 5.1 for comparison.

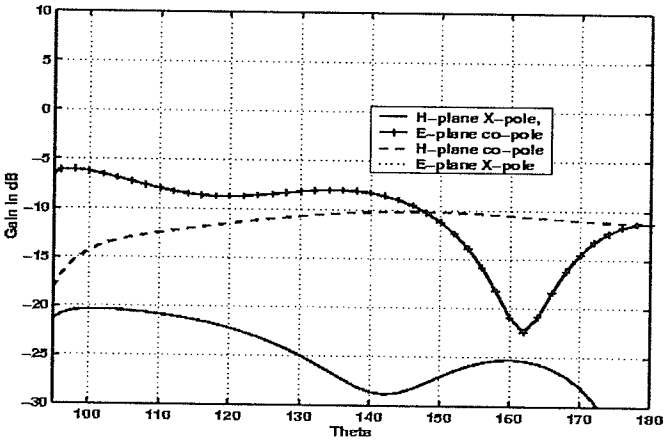

Fig. 5.7 (a) Back radiation from the reference patch shown in Fig. 5.3

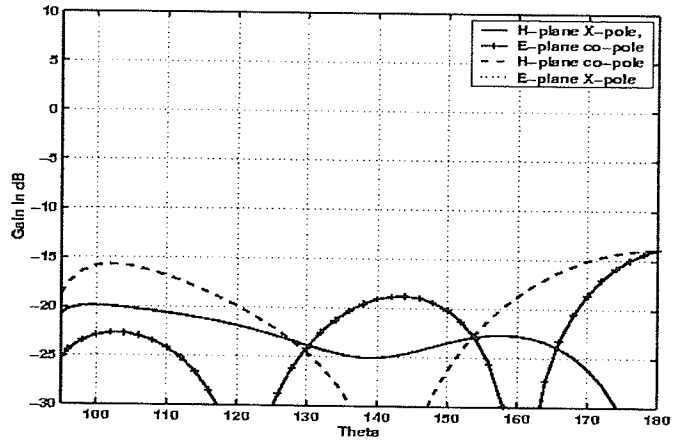

Fig. 5.7 (b) Back radiation from the PBG patch shown in Fig. 5.6

Table 5.1 Comparison of the resonant frequency, gain, and half power beamwidth of the reference and PBG patch antennas with L = 14 mm, W = 20 mm, ε_r = 3.2, h = 1.59 mm

	f_r (GHz)	Gain at $\theta = 0$ (dB)	HPBW (E-plane) (degrees)	HPBW (H-plane) (degrees)
Reference Antenna	5.6	5.3	131	73
PBG Antenna	5.78	9.6	55.2	69.8

To see the effects of the PBG position on the performance of the antenna, the PBG structure shown in Fig. 5.5 was moved away from the patch and the results on the resonant frequency, gain and half power beamwidths as a function of distance Y′ and X′ were recorded. The results are shown in Table 5.2.

Table 5.2 Resonant frequency, gain, and half power beamwidth for the patch antenna with L = 14 mm, W = 20 mm, ε_r = 3.2, h = 1.59 mm as a function of distance X' and Y'

Distance (Y') (mm)	***Distance (X') (mm)***	***f_r (GHz)***	***Gain at $\theta = 0$ (dB)***	***HPBW (E-plane) (degrees)***	***HPBW (H-plane) (degrees)***
8.3	12.4	5.78	9.6	52.8	73
12.3	16.4	5.64	8.87	60	74
16.3	20.4	5.6	7.64	79	78
20.3	24.4	5.56	5.56	142	82
24.3	28.4	5.45 5.61	4.82 4.9	146 142	66 71

From table 5.2, it is evident that by moving the PBG structure away from the patch antenna, the half power beamwidth in the E-plane increases significantly and at one point the E-plane and the H-plane patterns overlap. Since the half power beamwidths increase there is a drop in the gain of the antenna. The resonant frequency of the antenna also shifts down and eventually reaches the resonant frequency of the reference patch antenna as expected.

In addition to the 8 mm by 8 mm PBG patch structure, the 6 mm by 6 mm PBG structure was also placed around the antenna operating at 5.6 GHz. The RCS for the 6 mm by 6 mm PBG structure was shown in Fig. 5.2. This structure had a bandgap between 6.25 to 8.5 GHz and another between 10.25 to 14.75 GHz. However, at 5.6 GHz there was no reflection of the TM wave and this was confirmed by the gain results of the antenna. After placing the PBG around the patch, there was no change in the gain pattern of the patch. In fact, the pattern was identical to that of the reference patch antenna with no

PBG. To see the effects of the finite ground plane size on the radiation pattern of the PBG patch, different ground plane sizes were simulated. The effects of the ground plane size on microstrip patch antennas have been studied previously by S. Noghanian and L. Shafai [32]. It has been shown that by changing the size of the ground plane one can increase the gain of an antenna and control the beamwidth of the E and H plane patterns. By choosing the proper size of ground plane, the E and H plane co-polar patterns can be modified such that an overlap of the patterns is made possible [32]. However, for the PBG patch antenna shown in Fig. 5.6, the size of the finite ground plane was not effective in radiation patterns of the antenna. The antenna with PBG was placed on different finite ground planes, and the ground plane size was varied between 0.5λ to 2λ. The variation of the ground plane size did not have much effect on the beamwidth of the E and H planes, and very small variations in the antenna gain at $\theta = 0$ was noticed.

In addition to a finite ground plane, an infinite ground plane was also used in the simulations. The use of PBG around the patch on an infinite ground plane did not improve the radiation pattern of the patch.

Next, the second patch with dimensions of L = 7 mm and W = 12 mm was simulated with the PBG structure. However, since this patch operates at 10.95 GHz, the PBG structure used had to be modified to create a stopband at the patch resonance. For this case a PBG with metal patches of dimensions 4 mm by 4 mm and spacing of 0.2 mm was used. The vias for this case are the same as before with a diameter of 1.2 mm. The RCS for this structure is shown in Fig. 5.8.

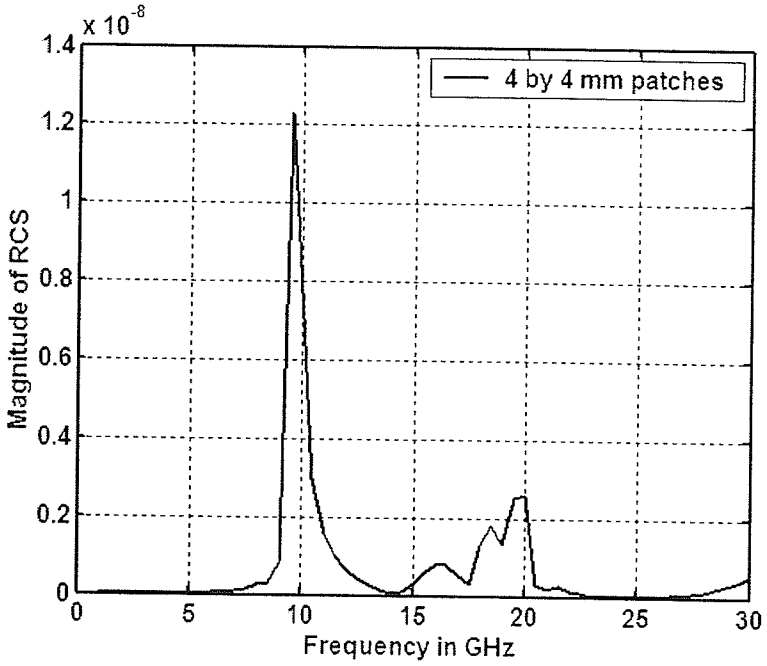

Fig. 5.8 Magnitude of RCS vs. frequency for the PBG on substrate with ε_r = 3.2 and h = 1.59 mm,(wave incident horizontally)

A few different PBG configurations were simulated with this antenna. For the first case, the geometry shown in Fig. 5.5, was simulated. The reflection coefficient of the PBG antenna showed a reduction in its -10 dB bandwidth, as well as a shift of the resonant frequency to 11.8 GHz, from 10.95 GHz of the reference antenna. The radiation patterns of this structure are shown in Fig. 5.9. Comparing these pattern to those shown in Fig. 5.4, it is observed that the gain has increased from 4 dBi to 8 dBi. In addition, the dip in the E-plane co-polar pattern has disappeared. The back radiation has also dropped significantly compared to that of the reference patch. Once again, the increase in the cross-polar levels can be reduced by moving the PBG structure away from the patch in the x direction, like the previous case.

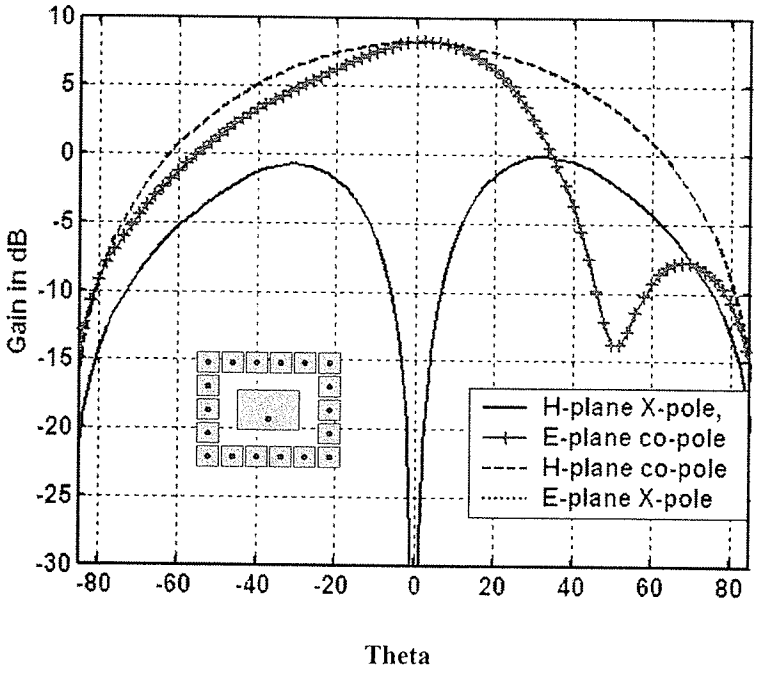

Fig. 5.9 E and H plane patterns of the PBG patch with L = 7 mm, W = 12 mm, ε_r = 3.2, h = 1.59 mm, X' = 8.5 mm Y' = 6.4 mm at 11.8 GHz

Figure 5.10 shows another configuration which was simulated.

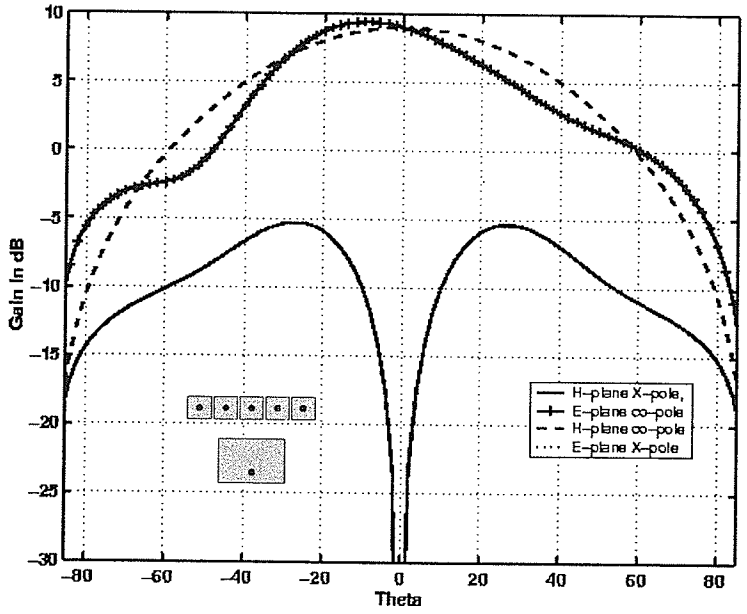

Fig. 5.10 E and H plane patterns of the PBG patch with a single row of metallic patches, L = 7 mm, W = 12 mm, ε_r = 3.2, h = 1.59 mm, Y' = 6.4 mm at 11.22GHz

The configuration shown in Fig. 5.10 increased the gain even higher to 9 dB and reduced the cross-pole to a lower level than the one shown in Fig. 5.9.

In addition to the 4 mm by 4 mm PBG structure used in the above antenna, the structure with dimensions of 8 mm by 8 mm was also tested with the above antenna. Looking back at the RCS of the 8 mm by 8 mm PBG structure, shown in Fig. 5.2, a second reflection between 8 to 11.75 GHz is observed. Therefore, one could use this configuration to stop the TM waves and hence improve the performance of the patch antenna operating in this range. Using the 8 mm by 8 mm PBG, the antenna gain with the radiation pattern shown in Fig. 5.4, increased to 8 dB and the dip in the E-plane pattern disappeared. The resonant frequency of the patch in this case was not affected by the use of PBG. The gain of this antenna is shown in Fig. 5.11.

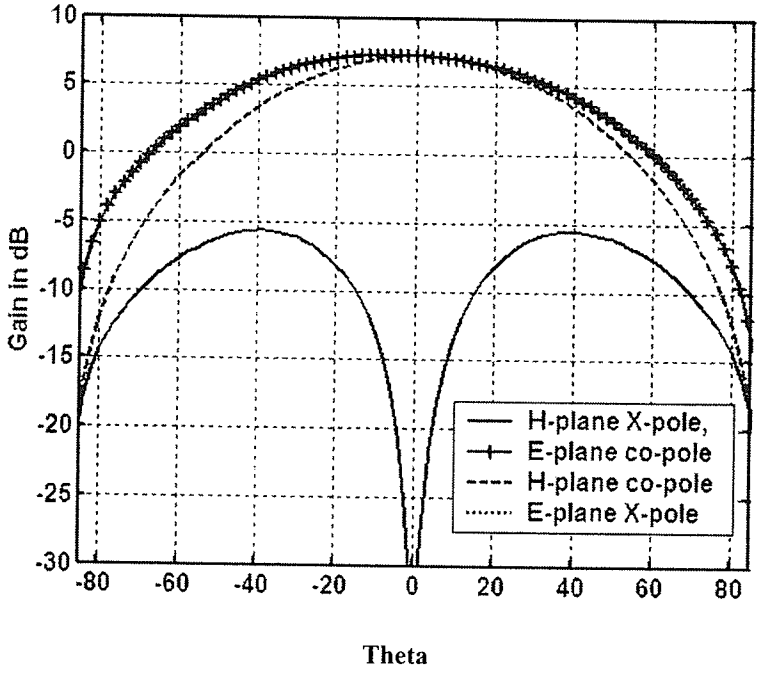

Fig. 5.11 E and H plane patterns of the patch with 8 mm by 8 mm PBG structure
$L = 7$ mm, $W = 12$ mm, $\varepsilon_r = 3.2$, $h = 1.59$ mm, $X' = 8.4$ mm $Y' = 8.4$ mm at 11.22GHz

The antennas shown in this section were fabricated and tested at the Antenna Laboratory of the University of Manitoba. The measurement results of these antennas are shown in the next chapter along with the reflection coefficients obtained from simulations.

5.2.2 Patch Antenna on $\varepsilon_r = 2.5$ PBG Substrate

For this section, different patch antennas with PBG on a substrate with permittivity of 2.5 were simulated. The PBG used on this substrate had metal patches of dimensions 8 mm by 8 mm and spacing of 0.2 mm. The vias used were the same as before with a diameter of 1.2 mm. The RCS for this particular PBG is shown in Fig. 5.12, and shows a peak reflection between 5 to 7 GHz. Therefore, the patch is designed to operate in this frequency range.

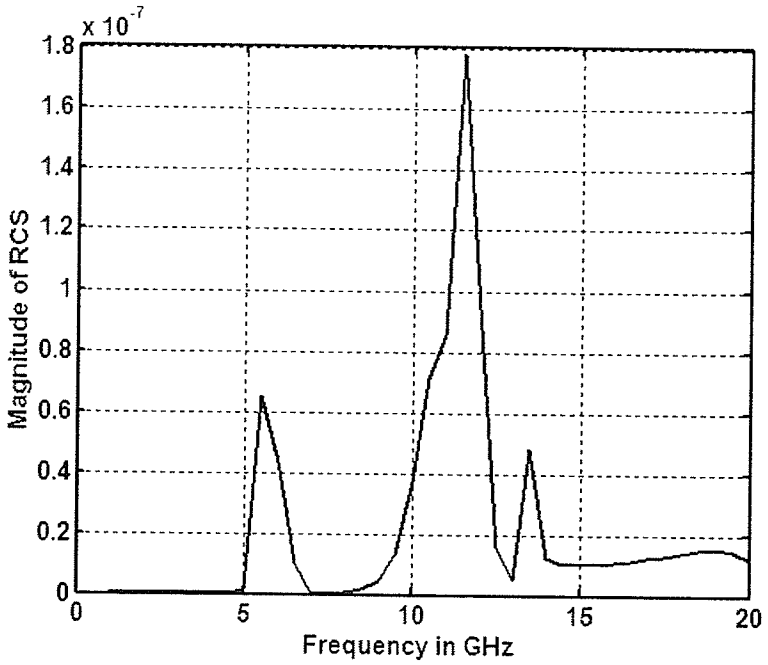

Fig. 5.12 Magnitude of RCS vs. frequency for the PBG on a substrate with $\varepsilon_r = 2.5$ and $h = 1.59$ mm, (wave incident horizontally)

The particular patch simulated with the above PBG has a length of 15.4 mm and a width of 22 mm. The patch is probe fed and the substrate height is 1.59 mm. The S_{11} for this antenna is shown in Fig. 5.13. As it can be seen the patch resonance is at 5.77 GHz, which is in the desired frequency range of the PBG structure.

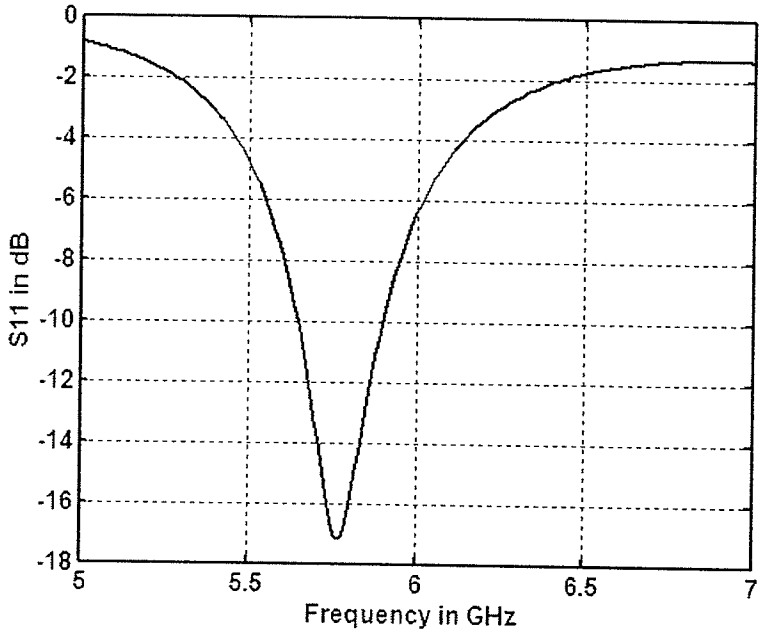

Fig. 5.13 The S_{11} for the reference patch with dimensions L = 15.4 mm, W = 22 mm, ε_r = 2.5, h = 1.59 mm

The radiation patterns of this patch at 5.77 GHz are shown in Fig. 5.14. Once again a wide E-plane co-polar pattern with a dip at $\theta = 0$ is observed.

Next, the PBG structure with RCS shown in Fig. 5.12 was placed around the patch antenna. The PBG was placed at a distance X′ = 12.4 mm and Y′ = 8.3 mm. By placing the PBG around the antenna, antenna resonance shifted to a higher frequency of 6.27 GHz as shown in Fig. 5.15. Comparing the S_{11} of the PBG antenna to that of the reference antenna shown, in Fig. 5.13, a reduction in the -10 dB bandwidth is noticed.

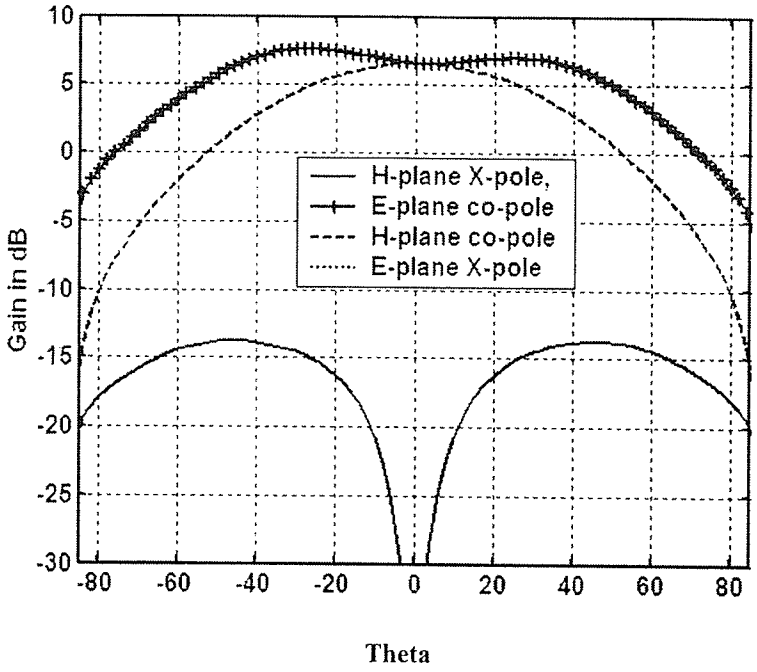

Fig. 5.14 E and H plane patterns of the reference patch with L = 15.4 mm, W = 22 mm, ε_r = 2.5, h = 1.59 mm

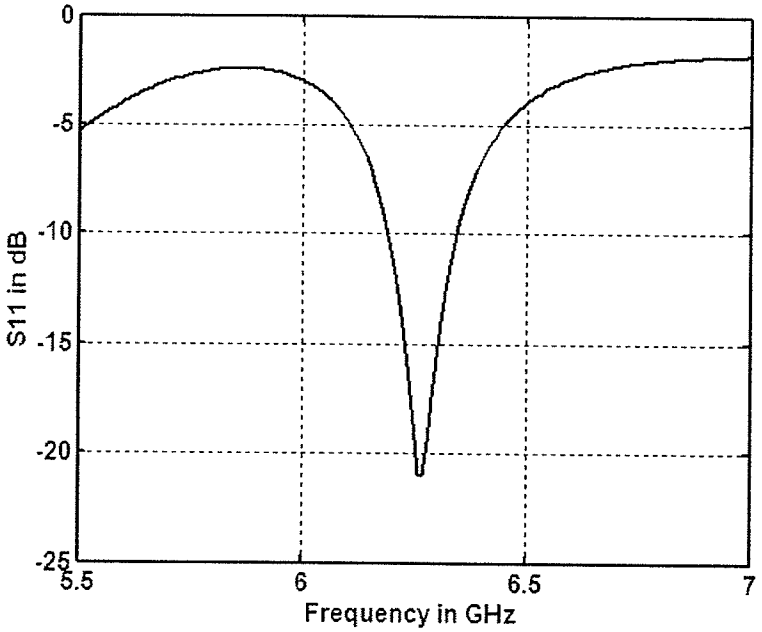

Fig. 5.15 The S_{11} for the PBG patch with dimensions L = 15.4 mm, W = 22 mm ε_r = 2.5, h = 1.59 mm, X′ = 12.4 mm, Y′ = 8.3 mm

The radiation pattern of this antenna was also plotted and shown in Fig. 5.16. The radiation pattern showed significant improvement in the gain at $\theta = 0$. The gain increased from 5.77 dBi of the reference patch to 10.33 dBi. The E-plane co-polar pattern also became narrower than the H-plane co-polar pattern and the amount of back radiation at θ = 100 degrees dropped significantly from -5 dB to -16 dB. The backlobe radiation of the PBG and reference patch antennas are compared in Fig. 5.17a and b respectively.

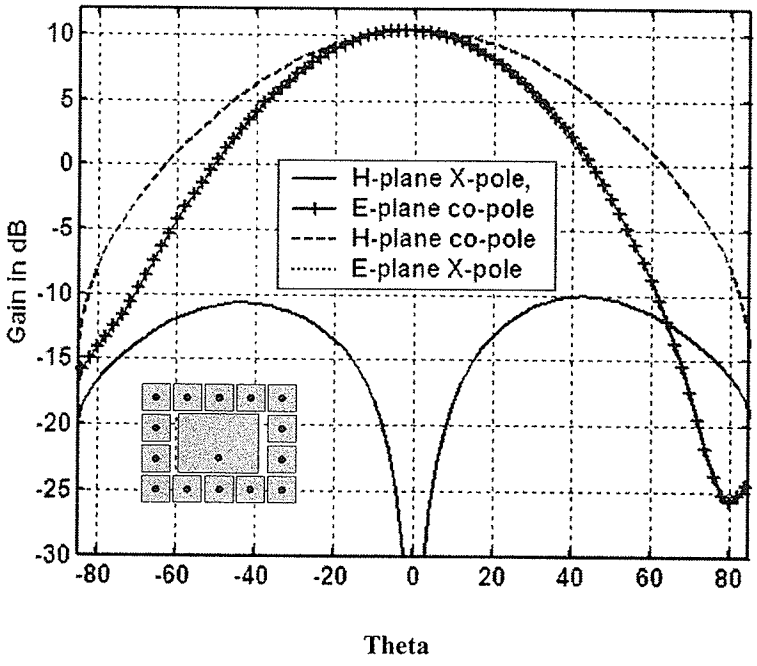

Fig. 5.16 E and H plane patterns of the PBG patch with
L = 15.4 mm, W = 22 mm, ε_r = 2.5, h = 1.59 mm, X' = 12.4 mm, Y' = 8.3 mm

The resonant frequency, gain, and half power beamwidths of the reference patch and the PBG patch antennas are given in Table 5.3 for comparison.

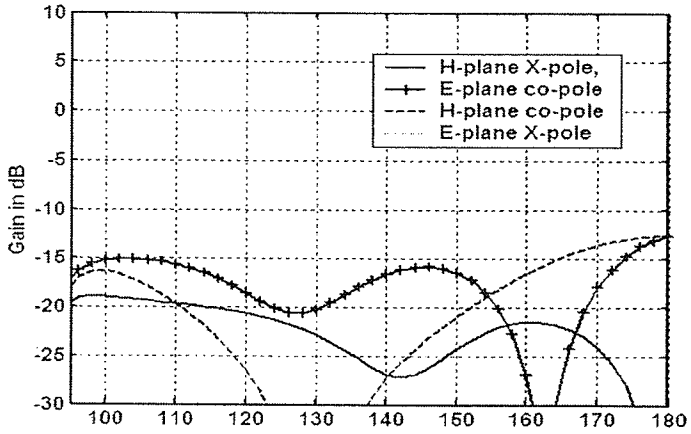

(a)

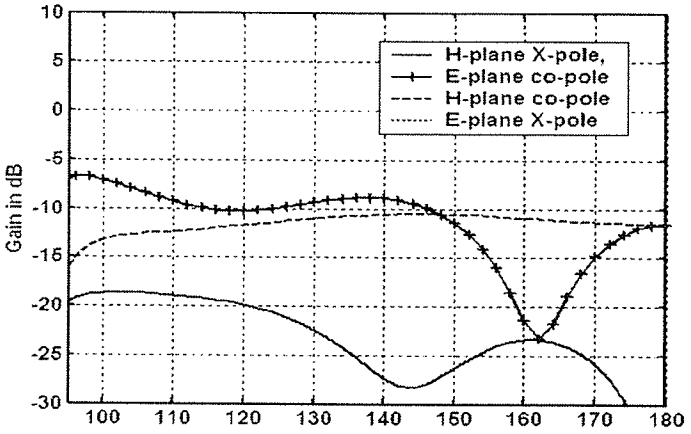

(b)

Fig. 5.17 (a) Back radiation from the reference patch shown in Fig. 5.14
(b) Back radiation from the PBG patch shown in Fig. 5.16

Table 5.3 Resonant frequency, gain, and half power beamwidth for the patch with $L = 15.4$ mm, $W = 22$ mm, $\varepsilon_r = 2.5$, $h = 1.59$ mm

	f_r (GHz)	Gain at $\theta = 0$ (dB)	HPBW (E-plane) (degrees)	HPBW (H-plane) (degrees)
Reference Antenna	5.77	6.58	118	72
PBG Antenna	6.27	10.33	52	69

To see the effects of PBG structure position on the performance of the patch, the PBG was moved away from the patch and this caused a reduction in the gain and an increase in the half power beamwidth of the E plane co-polar pattern as expected. The resonant frequency also shifted down toward that of the reference patch.

5.2.3 Patch Antenna on $\varepsilon_r = 1.0$ PBG Substrate

The use of PBG on foam ($\varepsilon_r \approx 1$) did not have any effect on the performance of the patch. Different PBG structures with various dimensions were tested around microstrip antenna on foam. However, non of the structures caused a change in the performance of the patch antenna.

5.2.4 Patch Antenna on $\varepsilon_r = 9.8$* PBG Substrate

The substrate material with ε_r 9.8 is covered in this section because of problems encountered in the simulations using Ensemble. Due to high permittivity and complexity of the structures used in the simulations, there were discrepancies in the gain results obtained from Ensemble. For certain structures, the differences in the gain values sometimes reached as high as 6 dB. The discrepancies in the gain values were mainly due to meshing of the structure under test.

To solve for the far fields numerically, the software breaks the structure down into small sections and for each section the currents on the structure along with the far fields and near fields are calculated. If the meshing of the structure is to complex (i.e. High frequency meshing), the calculated results will be inaccurate. Therefore, when testing

complicated structures, the proper meshing frequency has to be used in order to have dependable results. For all the simulation results in this section, a fixed mesh at 2 GHz is used for gain calculations. The gain values obtained are confirmed with their half power beamwidths for each simulation.

The first structure simulated in this section is a probe fed patch on a substrate material with a thickness of 1.59 mm. The patch antenna used has a length of 14 mm and a width of 20 mm. The size of the ground plane is 80 mm by 80 mm and the patch resonant frequency is at 3.24 GHz. The S_{11} for this patch is shown in Fig. 5.18.

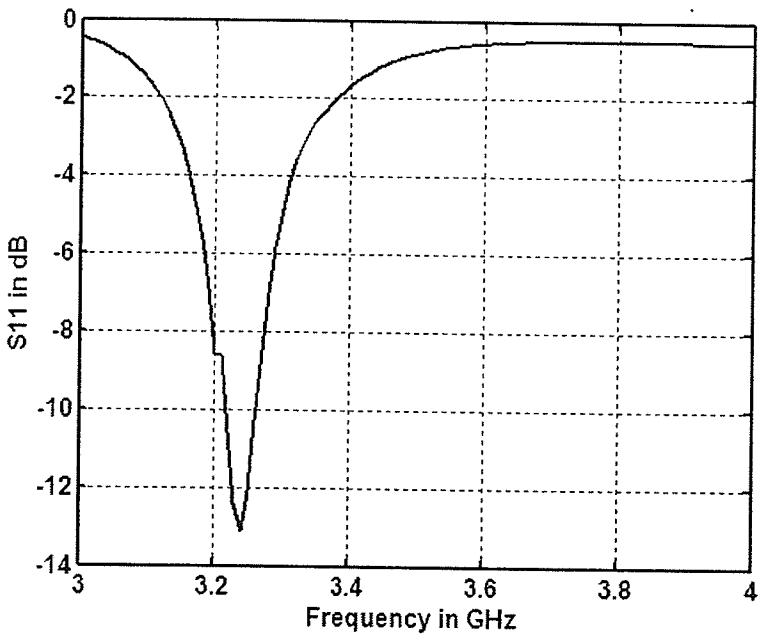

Fig. 5.18 The S_{11} for the reference patch with dimensions L = 14 mm, W = 20 mm, ε_r = 9.8, h = 1.59 mm

The radiation patterns of this patch are shown in Fig. 5.19. Its gain at $\theta = 0$ is 4.54 dBi and once again the E-plane co-polar pattern is observed to be wider than the H-plane

co-polar pattern. There is also a large amount of back radiation from the finite ground plane, which will be shown later.

Next, a PBG structure with metal patches of dimensions 8 mm by 8 mm and spacing of 0.2 mm was placed around the patch antenna. The vias used for this PBG have a diameter of 1.2 mm. The RCS for this PBG structure is shown in Fig. 5.20. As it can be, seen there is a peak reflection between 3 and 5.1 GHz for the TM mode.

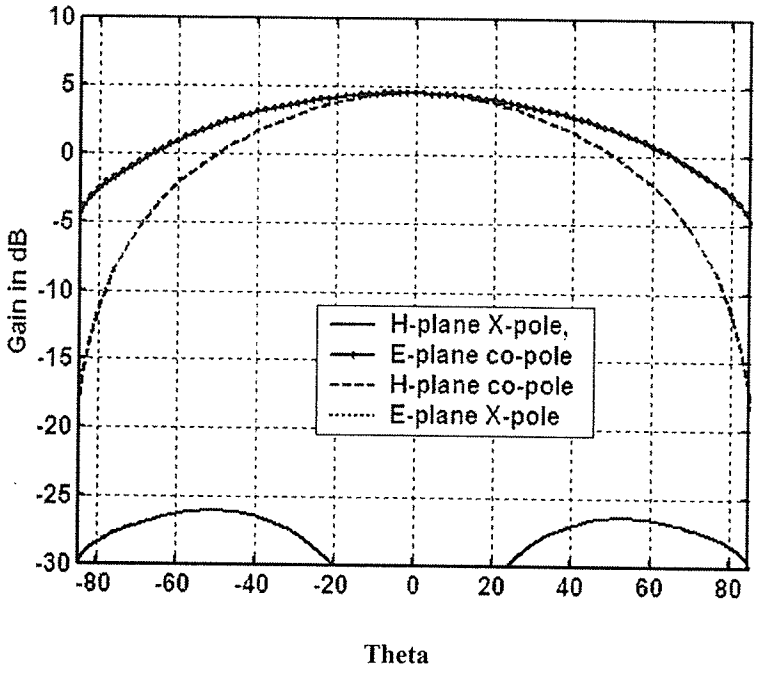

Fig. 5.19 E and H plane patterns of the reference patch with L = 14 mm, W = 20 mm, ε_r = 9.8, h = 1.59 mm

Once the RCS of the PBG was obtained, the structure was placed around the patch antenna shown above and the results on the resonant frequency, gain and half power beamwidth were recorded. The S_{11} of the PBG patch antenna is shown in Fig. 5.21. From the S_{11} plot it can be seen that there are two resonances for this structure. The first occurs at 3.09 GHz while the second occurs at 3.35 GHz.

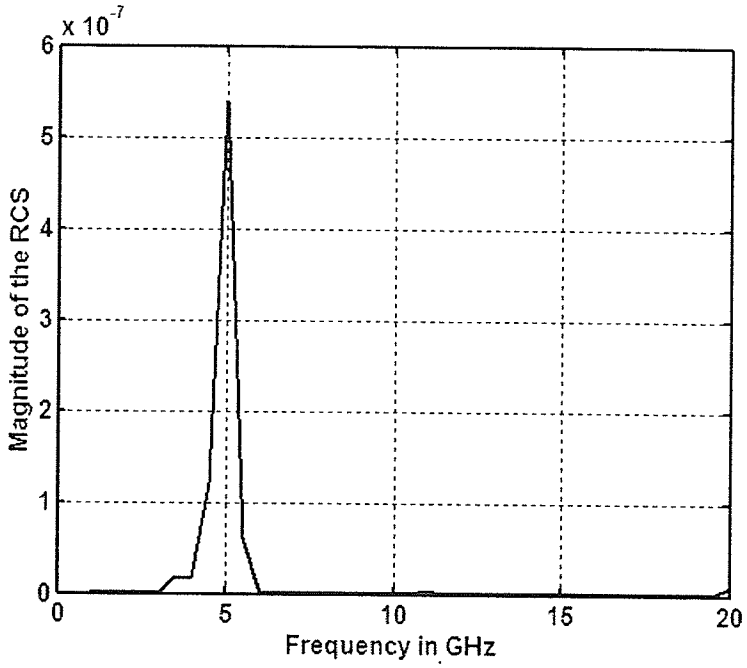

Fig. 5.20 Magnitude of RCS vs. frequency for the PBG on a substrate with ε_r = 9.8 and h = 1.59 mm,(wave incident horizontally)

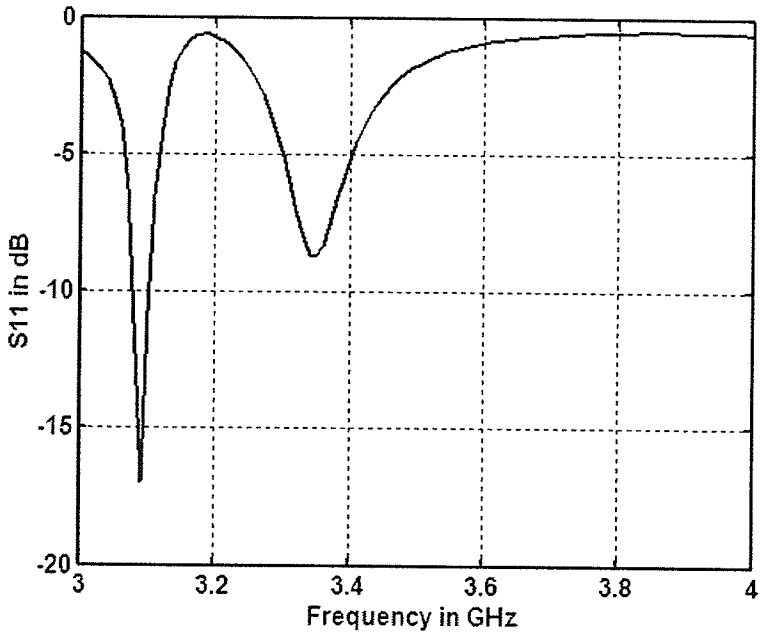

Fig. 5.21 The S_{11} for the PBG patch with dimensions L = 14 mm, W = 20 mm, ε_r = 9.8, h = 1.59 mm X′ = 12.4 mm, Y′ = 8.3 mm

Both minima in Fig. 5.21 are for the dominant mode and hence have the same polarization. However, the first mode at 3.09 GHz has a gain of 3 dBi and a very wide E-plane co-polar pattern. The second mode at 3.35 GHz showed an increase in the gain at $\theta = 0$ to 5.38 dBi compared with 4.54 dB of the reference patch.

The radiation patterns for this frequency are shown in Fig. 5.22. The increase in gain at this frequency was expected since the PBG has the effect of shifting the resonance to a higher frequency, compared with the reference antenna. It should be noted that for this frequency, the E plane co-polar pattern remained wider than the H plane co-polar pattern which was not expected.

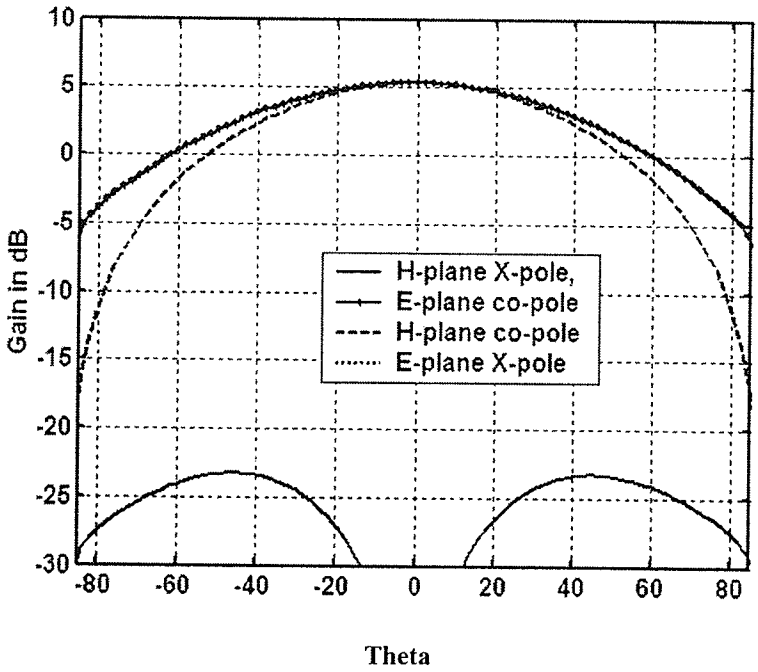

Fig. 5.22 E and H plane patterns of the PBG patch with
$L = 14$ mm, $W = 20$ mm, $\varepsilon_r = 9.8$, $h = 1.59$ mm, $X' = 12.4$ mm, $Y' = 8.3$ mm

Table 5.4 shows the resonant frequency, half power beamwidth and maximum gain for the reference and the PBG patch antennas.

Table 5.4 Resonant frequency, gain, and half power beamwidth for the patch with $L = 14$ mm, $W = 20$ mm, $\varepsilon_r = 9.8$, $h = 1.59$ mm

	f_r (GHz)	Gain at $\theta = 0$ (dB)	HPBW (E-plane) (degrees)	HPBW (H-plane) (degrees)
Reference Antenna	3.24	4.54	109	82
PBG Antenna	3.35	5.38	91	80

In addition to a single layer, a double layer PBG structure, Fig. 5.24, was also simulated. The additional layer in this case showed further increase in the gain of the patch, compared to a single layer PBG (shown in Fig. 5.22). The resonant frequency and the gain of this antenna are shown in Figs. 5.23 and 5.24 respectively.

From the S_{11} plots it can be seen that there are three minima in the reflection coefficient of the antenna. The first minimum at 3.1 GHz has a gain of 1.9 dBi at $\theta = 0$ and the second minimum at 3.2 GHz has a gain of 3.2 dBi. As one might expect, the third minimum at 3.37 GHz has the highest gain of 6.9 dBi. The three minima are for the same modes with the same polarizations. The geometry of this antenna along with the radiation patterns at 3.37 GHz are shown in Fig. 5.24.

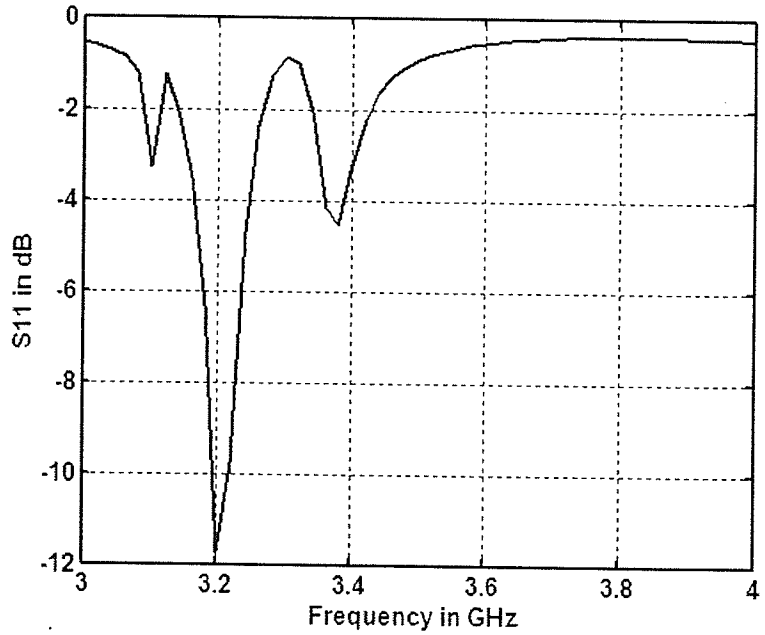

Fig. 5.23 The S_{11} for the PBG patch with 2 PBG layers and dimensions L = 14 mm, W = 20 mm, ε_r = 9.8, h = 1.59 mm X′ = 12.4 mm, Y′ = 8.3 mm

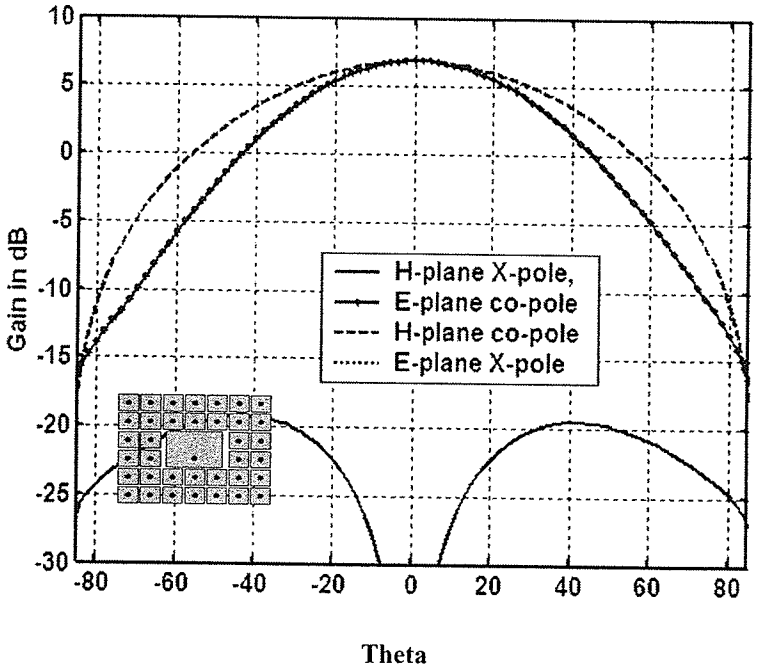

Fig. 5.24 E and H plane patterns of the PBG patch with 2 layers of PBG, L = 14 mm, W = 20 mm, ε_r = 9.8, h = 1.59 mm, X′ = 12.4 mm, Y′ = 8.3 mm at 3.37 GHz

For comparison, the back lobe radiation patterns of this antenna and the reference antenna in Fig.5.19 are shown in Fig. 5.25 (a) and (b) respectively. From the plots it can be seen that the back radiation level of the PBG patch are reduced significantly, compared with that of the reference antenna. There is a reduction of up to 15 dB at $\theta = 95$ degrees for the PBG antenna with 2 layers of PBG.

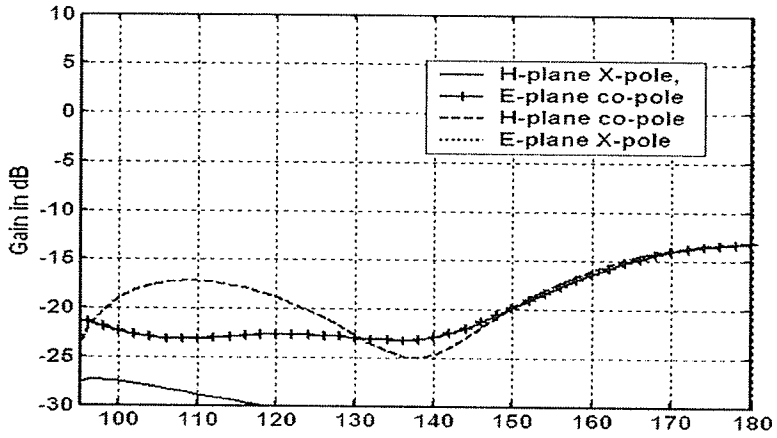

(a)

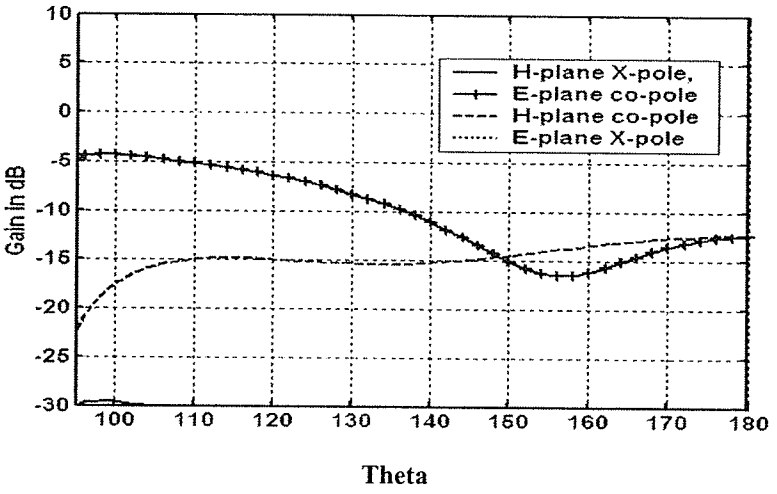

(b)

Fig. 5.25 (a) Back lobe radiation from the PBG patch shown in Fig. 5.24
(b) Back lobe radiation from the reference patch shown in Fig. 5.19

5.3 Conclusion

This chapter provided a study of high impedance photonic bandgap structures and their applications in microstrip patch antennas. In the first section, the basic background theory on the structures was reviewed along with the method used to measure the bandgap of the structures. The structures were used on different dielectric materials with relative permittivities ranging from 1.0 to 9.8. The bandgap of each PBG was measured by applying an incident wave to the structure and measuring the radar cross section of the TM wave vs. frequency. The peak in the RCS would define the bandgap of the structure. Next, the PBGs were placed around patch antennas on different substrate materials. The patch antennas were designed to operate at the frequency of the PBG bandgap. The use of PBG around the patch antennas increased the patch gain significantly by a factor of 3 to 4 times in special cases. The behavior of PBG was different for each substrate material. However, an overall increase in the antennas, gain along with improved radiation patterns was observed. In addition, the amount of back radiation for most antennas was reduced significantly. Side effects of using PBG include reduction of -10 dB bandwidth, as well as an increase in the cross polarization levels. The increase in the cross polarization levels was mainly due to the currents induced on the PBG metal patches. By moving the PBG structures away from the patch the cross polarization levels decreased. However, this reduced the gain of the antenna.

Chapter 6

Fabrication Results

In this chapter the measured data from the fabricated antennas are discussed and compared with the simulated results. All the fabricated antennas are on the substrate with permittivity of 3.2 and a thickness of 1.59 mm. For each antenna the S_{11} parameter along with the smith chart are measured using the network analyzer. The far field radiation patterns of the antennas are measured in the Antenna Laboratory of the University of Manitoba. For each antenna the half power beamwidth, gain, and resonant frequency are recorded and compared with simulation results. It should be noted that, the substrate material used in the fabrication of the antennas had a large loss tangent of around 0.014 at the frequency of 5.5 GHz (the substrate was sample sheets from a new manufacturer with a non-uniform permittivity profile). Therefore the measured gain results are expected to be lower, compared with the simulated results in the previous chapter. The simulations in the previous chapter were done on a substrate with a loss tangent of 0.0001. In this chapter the simulations are repeated with a loss tangent of 0.014. Setting the loss tangent to 0.014, causes a significant reduction in the gain of the antennas.

6.1 Results of Antenna #1

The first antenna fabricated had dimensions of L = 14 mm and W = 20 mm. The ground plane dimensions for the fabricated antennas were 80 mm by 76 mm. For the simulated antennas they were 80 mm by 80 mm. The measured reflection coefficient is

compared with the simulated one in Figs. 6.1 and 6.2, respectively.

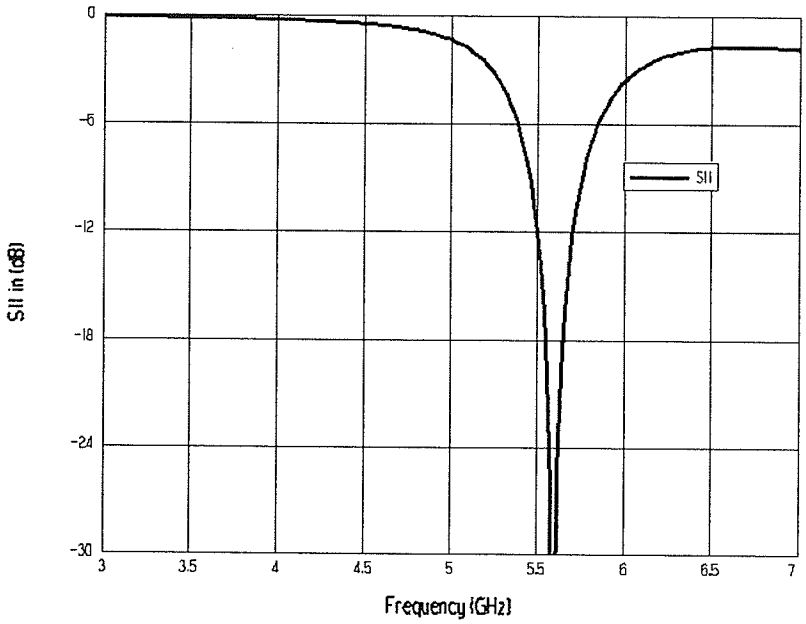

Fig. 6.1 S_{11} for the simulated patch with dimensions L = 14 mm, W = 20 mm, ε_r = 3.2, h = 1.59 mm

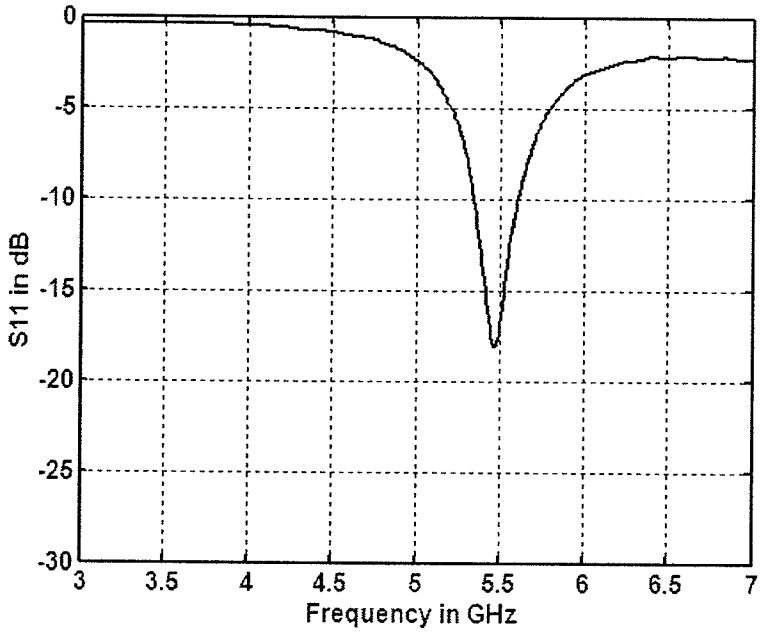

Fig. 6.2 S_{11} for the fabricated patch with dimensions L = 14 mm, W = 20 mm, ε_r = 3.2, h = 1.59 mm

Comparing the simulation results with those of the fabricated antenna, it can be seen that there is a slight shift in the resonant frequency which is to be expected. This shift in the resonant frequency can be due to many factors such as the size and position of the probe, the meshing of the simulated structure and the size of the ground plane.

Next, the smith chart for both simulated and fabricated antennas are shown in Figs. 6.3 and 6.4, respectively.

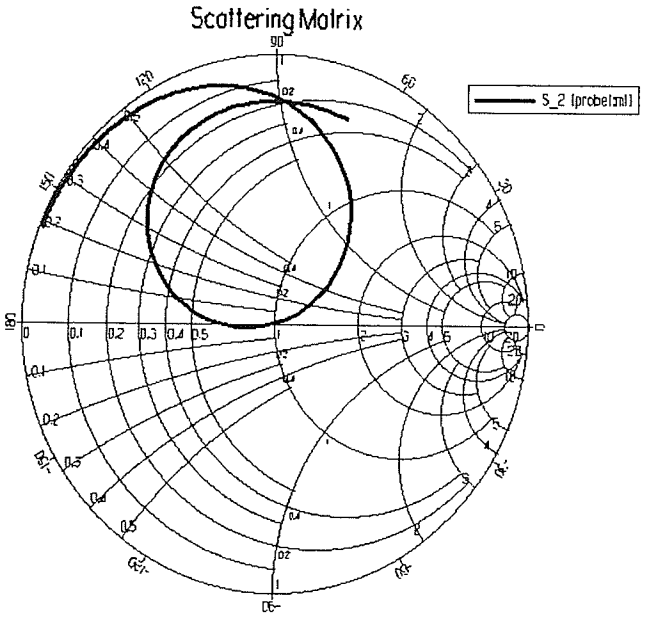

Fig. 6.3 The smith chart for the simulated patch with dimensions $L = 14\ mm, W = 20\ mm, \varepsilon_r = 3.2, h = 1.59\ mm$

Comparing Fig. 6.3 with Fig. 6.4, there is a slight shift in the impedance plot. This shift is due to the position of the reference plane. The shift in the reference plane creates a phase shift at the particular frequency of operation.

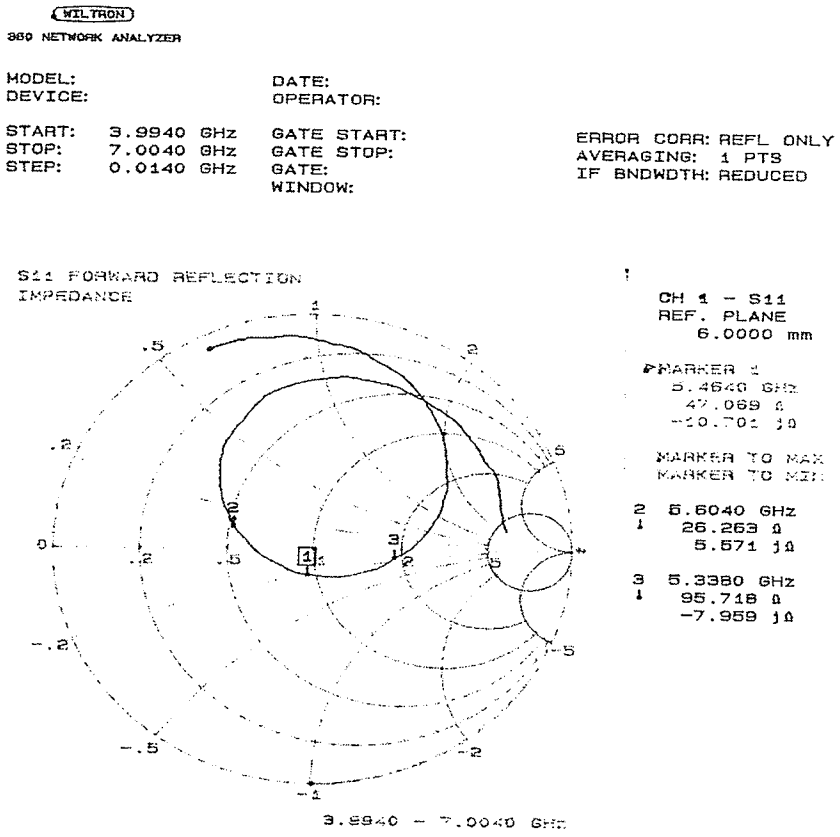

Fig. 6.4 The smith chart for the simulated patch with dimensions $L = 14$ mm, $W = 20$ mm, $\varepsilon_r = 3.2$, $h = 1.59$ mm

Next, the front and back radiations of the simulated antenna with the loss tangent taken into account is shown in Figs. 6.5a and b. Comparing the radiation patterns of this antenna with those shown in the previous chapter, Fig. 5.3, it can be seen that the loss tangent has a significant effect on the gain. There is a 1 dB reduction in gain. The measured E-plane and H-plane radiation patterns of this patch are shown in Figs. 6.6a and 6.6b, respectively. The co-polar patterns of the simulated antenna and the fabricated antenna are very similar. For both cases, the E plane co-polar pattern is wider than the H-plane co-polar pattern and a dip at $\theta = 0$ of the E-plane pattern is observed.

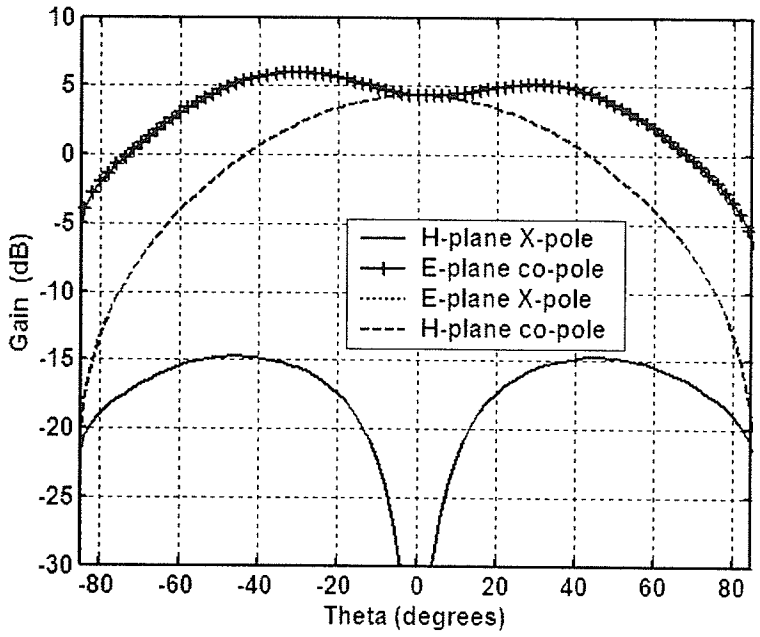

(a)

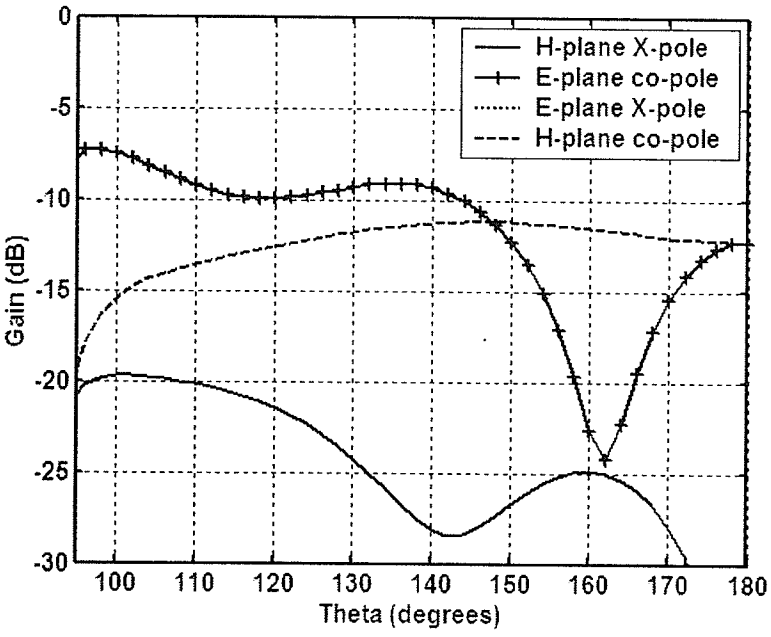

(b)

Fig. 6.5 E and H plane patterns of the simulated patch with L = 14 mm, W = 20 mm, ε_r = 3.2, tan δ = 0.014, h = 1.59 mm at 5.6 GHz (a) Front radiation (b) Back radiation

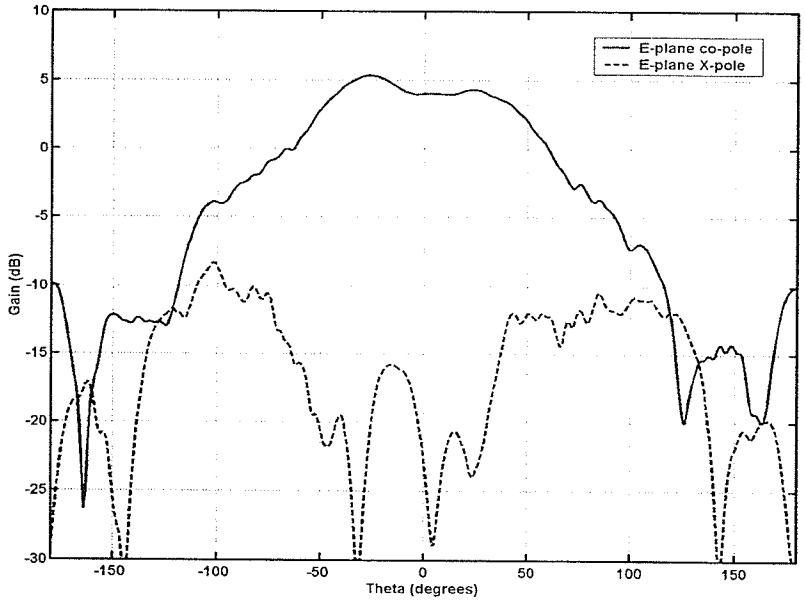

(a)

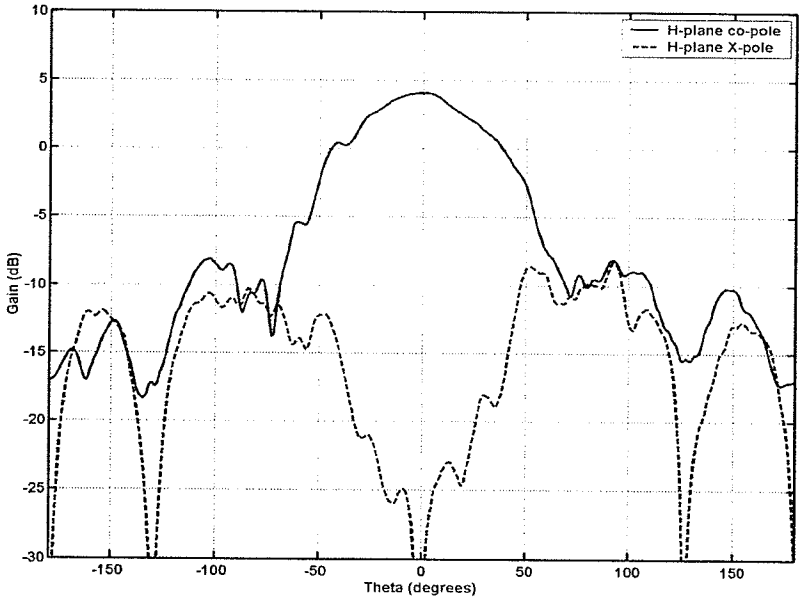

(b)

Fig. 6.6 Radiation patterns of the fabricated patch with L = 14 mm, W = 20 mm, ε_r = 3.2, h = 1.59 mm at 5.45 GHz (a) E-plane patterns (b) H-plane patterns

A gain of 4.09 dBi at $\theta = 0$ is obtained from the fabricated antenna, while the simulated antenna has a gain of 4.3 dBi at $\theta = 0$. The slight variations in the gain patterns can be due to different factors, such as the difference in the size of the ground planes, the meshing of the simulated antenna and the dielectric loss tangent of the substrate material.

6.2 Results of Antenna #2

In this section, antenna #1 with a PBG structures placed around it, Fig. 5.5, was fabricated and tested. The PBG consists of 8 mm by 8 mm metal patches and is located at a point with $X' = 12.4$ mm , $Y' = 8.3$ mm. The simulated reflection coefficient for this structure is shown in Fig. 6.7.

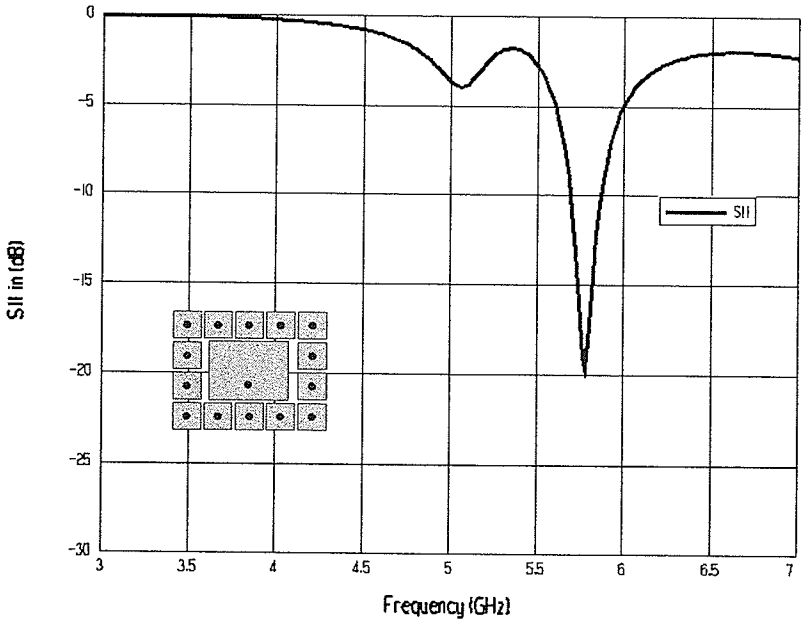

Fig. 6.7 S_{11} for the simulated PBG patch with dimensions $L = 14$ mm, $W = 20$ mm, $\varepsilon_r = 3.2$, $h = 1.59$ mm, $X' = 12.4$ mm , $Y' = 8.3$ mm

The reflection coefficient of the fabricated antenna is shown in Fig. 6.8. As it can be seen, there is a good agreement between the simulated and measured data. The smith

chart for the fabricated and simulated PBG patches are shown in Fig. 6.9 and Fig. 6.10, respectively.

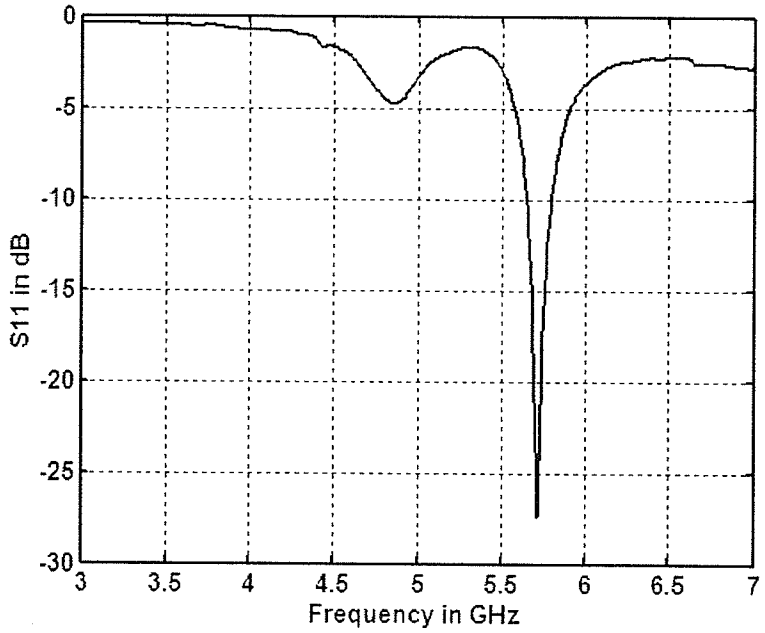

Fig. 6.8 Measured S_{11} for the fabricated PBG patch with dimensions L = 14 mm, W = 20 mm, ε_r = 3.2, h = 1.59 mm, X′ = 12.4 mm , Y′ = 8.3 mm

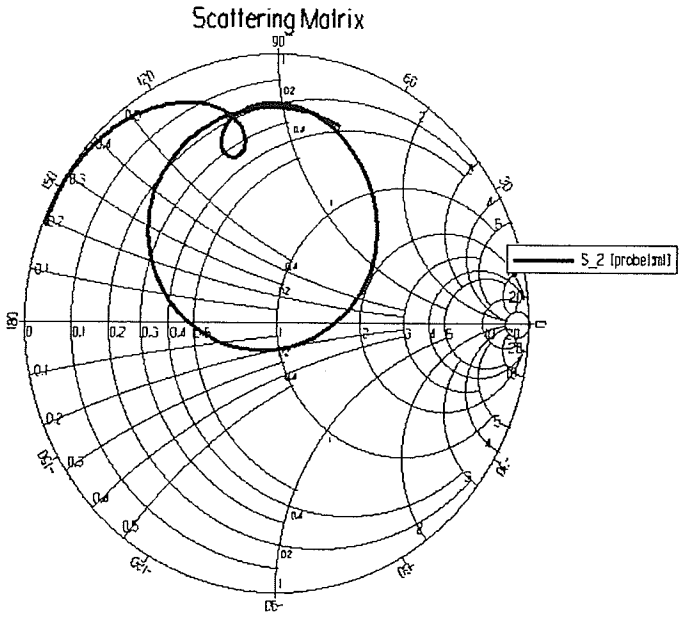

Fig. 6.9 The smith chart for the simulated PBG patch with dimensions L = 14 mm, W = 20 mm, ε_r = 3.2, h = 1.59 mm, X′ = 12.4 mm , Y′ = 8.3 mm

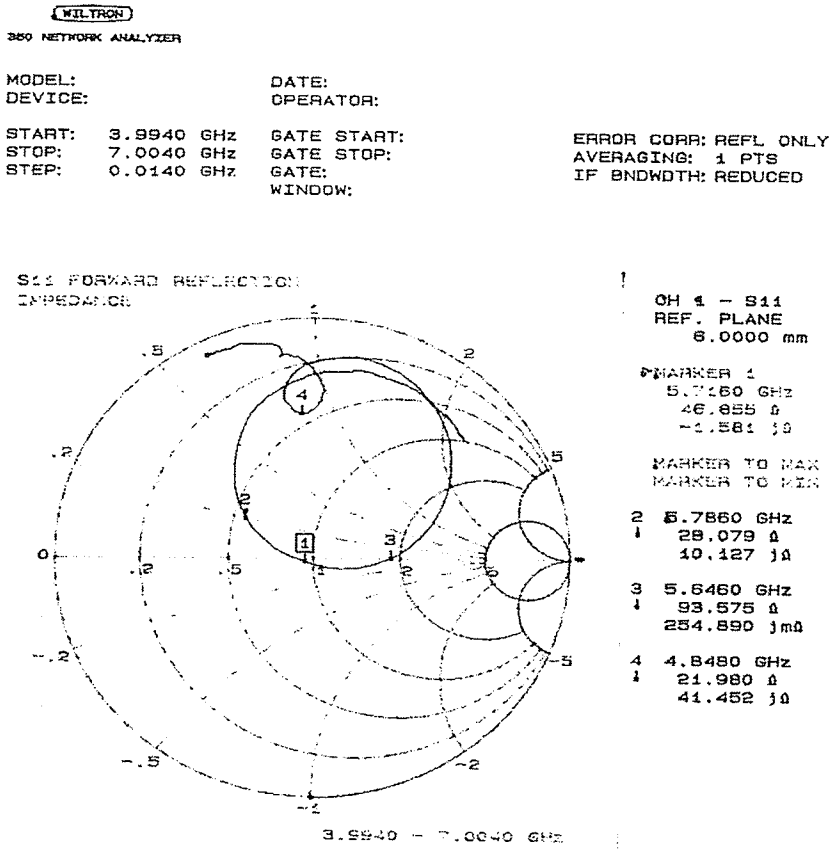

Fig. 6.10 The smith chart for fabricated PBG patch with dimensions L = 14 mm, W = 20 mm, ε_r = 3.2, h = 1.59 mm, X′ = 12.4 mm , Y′ = 8.3 mm

From the smith chart plots, it can be seen that there is very good agreement between the simulation and the fabrication results.

The simulated gain plots of the PBG antenna are shown in Fig. 6.11. As it can be seen, there is an increase in the gain of the antenna compared with the reference antenna shown in Fig. 6.5a. Comparing the gain plot, of the lossy substrate shown in Fig. 6.11, to the gain plot of the lossless substrate shown in chapter 5, Fig. 5.6, there is a decrease in the gain from 9.6 dBi to 7.76 dBi. The radiation patterns of the fabricated antenna are shown in Fig. 6.12a and 6.12b for the E-plane and the H-plane, respectively.

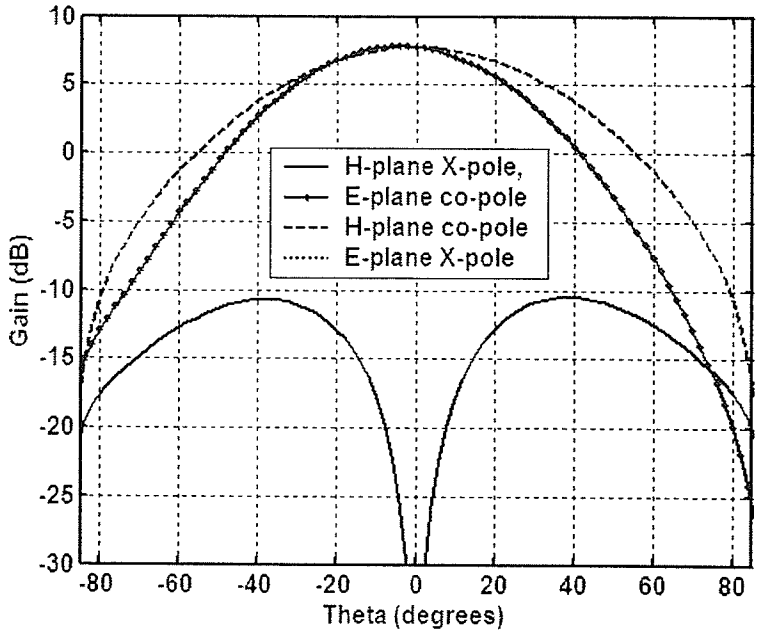

(a)

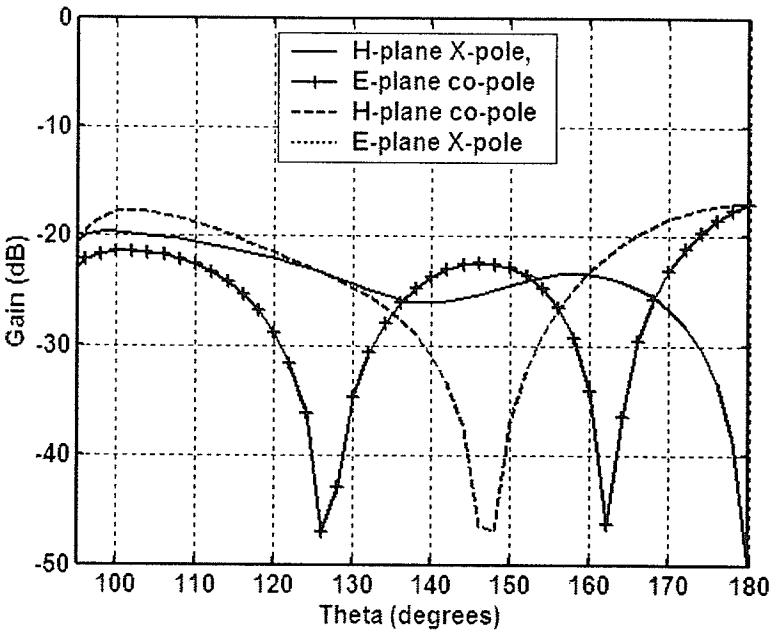

(b)

Fig. 6.11 E and H plane patterns of the simulated PBG patch with L = 14 mm, W = 20 mm, ε_r = 3.2, tan δ = 0.014, h = 1.59 mm, X′ = 12.4 mm , Y′ = 8.3 mm at 5.78 GHz (a) Front radiation (b) Back radiation

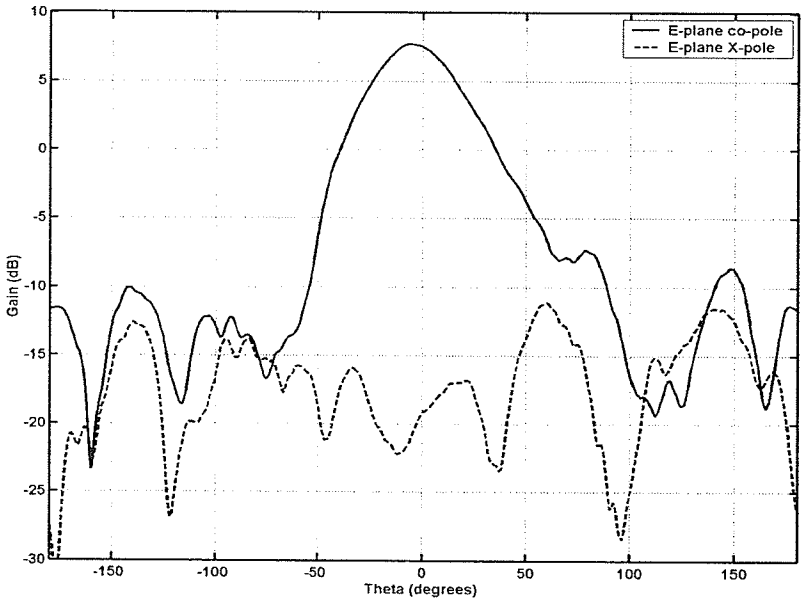

(a)

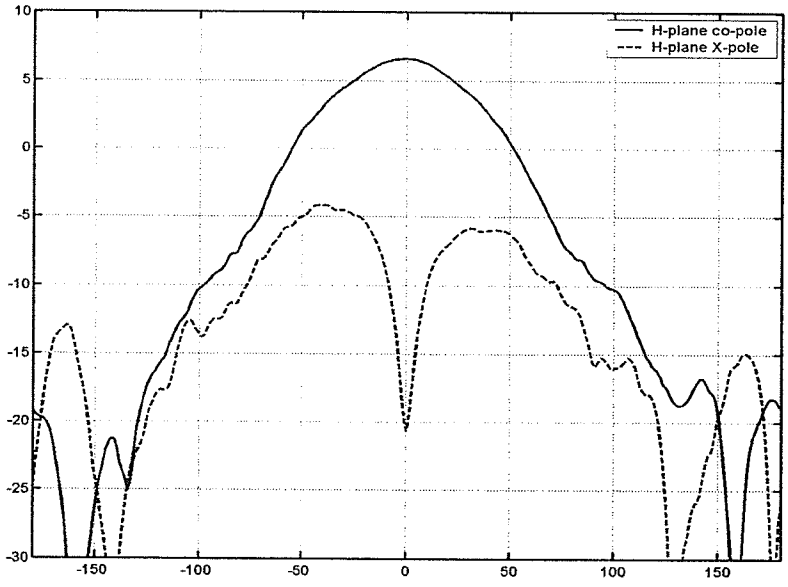

(b)

Fig. 6.12 Radiation patterns of the fabricated PBG patch with L = 14 mm, W = 20 mm, ε_r = 3.2, h = 1.59 mm, X′ = 12.4 mm , Y′ = 8.3 mm at 5.75 GHz (a) E-plane patterns (b) H-plane patterns

Comparing the fabricated gain plots to the simulated gain plots, the E-plane co-polar pattern is narrower than the H-plane co-polar pattern for both cases. The gain level at θ = 0 degrees for the fabricated antenna is 7.54 dBi which is very close to the simulated value of 7.76 dBi. A slight shift in the E-plane co-polar pattern is observed for both the simulated and the fabricated antennas. Overall, the cross polarization levels of the fabricated antennas are higher than the simulated values. This difference in the cross polarization levels could be due to the fabrication method or the meshing used in the simulations of the structure.

Comparing the fabricated reference and PBG antennas, the radiation patterns of the antenna with the PBG have improved significantly. The gain at θ = 0, of the antenna with the PBG has increased to 7.54 dBi from 4.09 dBi for the reference antenna. The E-plane co-polar pattern of the PBG is narrower than the H-plane co-polar pattern and the dip at θ = 0 of the E-plane has disappeared. In addition, the H-plane co-polar pattern is much smoother and the back radiation levels have dropped significantly.

The detrimental effects of using a PBG include a reduction in the -10 dB bandwidth from 4.83 % to 2.62 % and an increase in the cross polarization levels.

6.3 Results of Antenna #3

From the simulation results in chapter five it was found that by moving the PBG away from the patch the gain of the patch drops and eventually reaches that of the reference antenna with no PBG. In order to verify this, Antenna #2 with the PBG moved to position X′ = 24.4 mm, Y′ = 20.3 mm was fabricated and tested. The radiation patterns

of this antenna for the E plane and H plane are shown in Fig. 6.13a and 6.13b, respectively.

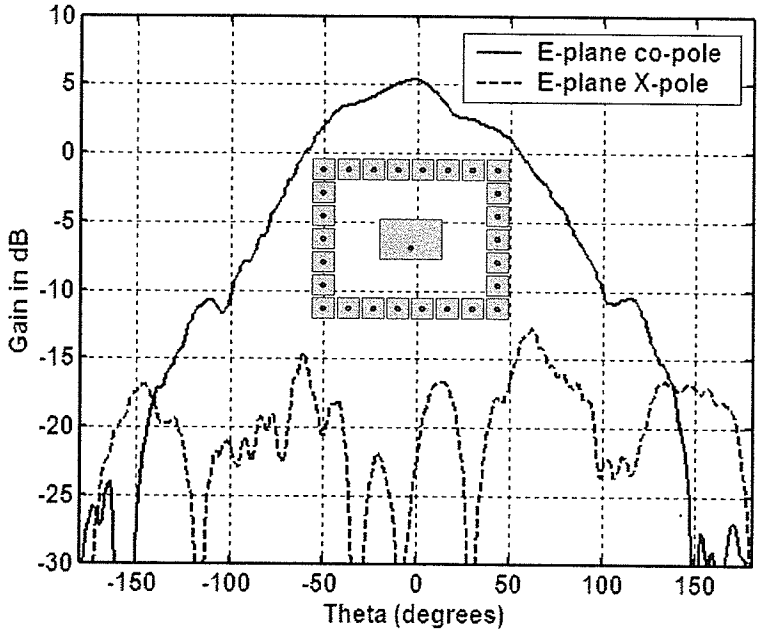

(a)

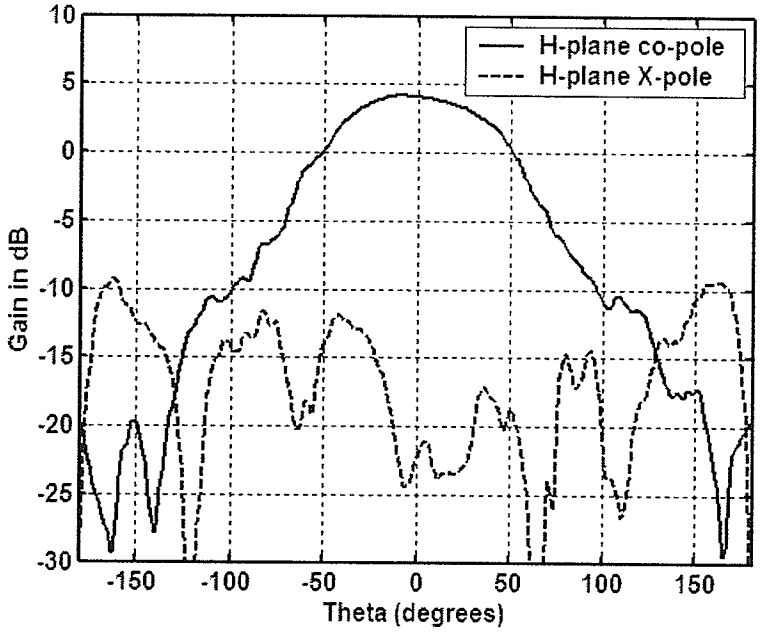

(b)

Fig. 6.13 Radiation patterns of the fabricated PBG patch with L = 14 mm, W = 20 mm, ε_r = 3.2, h = 1.59 mm, X′ = 24.4 mm , Y′ = 20.3 mm at 5.48 GHz (a) E-plane patterns (b) H-plane patterns

Comparing the radiation patterns of this PBG antenna to the reference antenna, i.e. Antenna #1, shown in Fig. 6.6, it is observed that the gain in the E-plane of the PBG antenna has increased slightly and the dip in the E-plane co-polar pattern has disappeared. The overall pattern of this antenna is smoother with much lower back radiation in both E and H planes. The cross-polar components of this antenna in both planes are similar to those of the reference antenna and have not changed significantly.

Due to the movement of the PBG structure away from the patch, the gain of this antenna is lower than Antenna #2. In addition, the E-plane co-polar pattern is wider than the H-plane co-polar pattern which, was to be expected. The sidelobe levels are also lower in the H-plane due to the large distance between the patch and the vias in the PBG.

Other antennas with PBG substrate at the frequency of 10.5 GHz were also fabricated. The use of PBG around the patch antennas increased the gain as expected. However, due to the high loss tangent of the substrate at 10.5 GHz, the gain levels were lower than expected.

6.4 Conclusion

This chapter provided a comparison of simulation results obtained from Ansoft Ensemble and measurement results obtained from the fabricated antennas. The antennas were fabricated on a substrate with a relative permittivity of 3.2 and a substrate height of 1.59 mm. The measured data from the fabricated antennas showed good agreement with the simulated data. The use of PBG substrate showed a remarkable improvement in the performance of the patch antenna both in the simulated and the fabricated results. In

addition, it was observed that by the use of a lossy substrate, the gain of the antenna drops by as much as 2 dBi which, is very significant.

In some cases, there were slight differences between the fabricated and simulated data. These differences are due to different factors such as the fabrication process and, the errors due to the meshing used in the simulations of the antennas.

Chapter 7

Conclusion

7.1 Summary

This thesis provided a comprehensive study of two dimensional PBG structures and their applications in microstrip transmission lines and patch antennas. The PBGs used in the designs and simulations can be summarized into two groups namely the Ground Plane PBGs and the High Impedance PBGs. The Ground Plane PBGs consisted of perforations in the ground plane of microstrip structures. The perforations were used in the ground plane of microstrip transmission lines to create filters from the line. It was shown that the properties of the filter are dependent on the period, geometry and size of the perforations. It was found that by using PBG structures of more than one period, a wideband filter with very low isolation levels, i.e. < -30 dB, can be created. The effective permittivity of the filters were found to be higher than those of a simple transmission line.

The perforations were also used in the ground plane of microstrip patch antennas. The perforations used included single hole, multiple holes and, slots in the ground plane. The perforations were implemented in the design of both narrowband and wideband patch antennas. For the narrowband patch antennas, the use of a single hole in the ground plane exhibited a decrease in the resonant frequency and an increase in -10 dB bandwidth of the patch. The perforations in the ground plane had the effect of decreasing the overall gain of the patch due to the increase in the back radiation. Placing a cavity underneath the antenna to reduce the back radiation, canceled the effects of the perforations.

In addition to a single hole, multiple holes were also implemented in the design of narrowband patch antennas. It was found that by the use of multiple holes and proper ground plane size, the excitation of higher order modes can be prevented. The excitation of higher order modes in a narrowband patch antenna can also be modified by etching slots in the ground plane. A shift in the resonance of higher order modes was achieved by placing slots in the ground plane along the length of the patch. The slots in the ground plane were also used in a wideband U-slot patch antenna to increase its -10 dB bandwidth.

The two dimensional High Impedance PBGs were also studied in this thesis. The bandgap of these PBGs were found by placing an incident wave on the structures and measuring the reflection of the TM wave as a function of frequency. The PBGs were then used in the design of patch antennas operating at different frequencies. The antennas with the PBGs were simulated on different dielectric materials. It was observed that by placing the PBGs around the patch, the gain of the patch can be increased by up to 3 to 4 times. In addition, smoother gain patterns with significant reduction in the back radiation were obtained.

The implementation of PBGs in the design of patch antennas had the effect of reducing the -10 dB bandwidth of the antennas and increasing the cross polarization levels. The increase in the cross polarization was caused by the currents flowing on the PBG structures. This increase was adjusted by moving the PBG away from the patch, which caused a reduction in the overall gain. It was also found that in most cases, a patch with a single layer of PBG has the best overall gain pattern. The use of multilayered PBG structures caused significant increase in the cross-polarization levels as well as distortion

in the co-polar gain patterns.

In order to confirm the simulation results, some of the antennas on the substrate with permittivity of 3.2 were fabricated and tested at the Antenna Laboratory of the University of Manitoba. The measured data showed excellent agreement with the simulated data.

7.2 Future Research

Below is a list of some suggestions for future work in the area of Photonic Bandgaps.

- A more detailed study of ground plane perforations to control the excitation of higher order modes in microstrip patch antennas.
- Reduction of the back radiation from the ground perforations without affecting the properties of the perforations.
- Use of ground plane perforations to further increase in the bandwidth of wideband patch antennas.
- Use of High Impedance PBGs in wideband and stacked patch antennas.
- Use of High Impedance PBGs in array applications to reduce the coupling effects between the adjacent elements and increase the overall gain of the array.
- Use of High Impedance PBGs in horn antennas to reduce the radiation from the surface currents flowing on the walls of the horn
- Use of High Impedance PBGs in the design of waveguides.

References

[1] F. Gardiol, "Microstrip Circuits", John Wiley & Sons, Inc. 1994.

[2] I.J. Bhahl, and P. Bhartia, "Microstrip Antennas", Artech House Inc. Dedham, Massachusetts, 1980.

[3] V. Radisic, Y. Quian, R. Coccioli, and T. Itoh, "Novel 2-D Photonic Bandgap Structure for Microstrip Lines", IEEE Microwave and Guided Wave Letters, Vol. 8, No. 2, Feb. 1998. pp. 69-71

[4] Y. Horii, and M. Tsutsumi, "Harmonic Control by Photonic Bandgap on Microstrip Patch Antenna", IEEE Microwave and Guided Wave Letters, Vol. 9, No. 1, Jan. 1999. pp. 13-15

[5] R. Gonzalo, P. de Maagt, and M. Sorolla, "Enhanced Patch-Antenna Performance by Suppressing Surface Waves Using Photonic-Bandgap Substrates", IEEE Transactions on Microwave Theory and Technique, Vol. 47, No. 11, Nov. 1999. pp. 2131-2138

[6] B. Elamaran, I. Chio, L. Chen, and J. Chiao, "A Beam-Steerer Using Reconfigurable PBG Ground Plane", IEEE MTT-S International Digest, Vol. 2, 2000, pp. 835-838

[7] F. R. Yang, K. P. Ma, Y. Qian, and T. Itoh, "A Uniplanar Compact Photonic-Bandgap (UC-PBG) Structure and It's applications for Microwave Circuits", IEEE Transactions on Microwave Theory and Technique, Vol. 47, No. 8, Aug. 1999. pp. 1509-1514

[8] Y. Qian, D. Sievenpiper, V. Radisic, E. Yablonovitch, and T. Itoh, "A Novel Approach for Gain and Bandwidth Enhancement of Patch Antennas", RAWCON Proceedings, 1998. pp. 221-224

[9] Y. Qian, R. Coccioli, D. Sievenpiper, V. Radisic, E. Yablonovitch, and I. Itoh, "A Microstrip Patch Antenna Using Novel Photonic Band-Gap Structures", The Microwave Journal, Jan. 1999. pp. 66-76

[10] D. Sienvenpiper, L. Zhang, R. F. Jimenez, N. G. Alexopolous, and E. Yablonovitch, "High-Impedance Electromagnetic Surfaces with a Forbidden Frequency Band", IEEE Transactions on Microwave Theory and Technique, Vol. 47, No. 11, Nov. 1999. pp. 2059-2074

[11] D. M. Pozar, "Microwave Engineering", John Wiley and Sons, Inc. 2nd edition, 1998.

[12] C. A. Balanis, "Antenna Theory Analysis and Design", John Wiley and Sons, Inc. 2nd edition, 1997.

[13] R. Coccioli, F. R. Yang, K. P. Ma, and T. Itoh, "Aperture-Coupled Patch Antenna on UC-PBG", IEEE Transactions on Microwave Theory and Techniques, Vol. 47, No. 11, Nov. 1999. pp. 2123-2130

[14] S. K. Sharma, and L. Shafai, "Enhanced performance of an aperture-coupled rectangular microstrip antenna on a simplified unipolar compact photonic bandgap (UC-PBG) structure", Antennas and Propagation Society, 2001 IEEE International Sym., Vol. 2 , 2001, pp. 498 -501

[15] Bhalla, R., and Shafai, L., "Resonance behavior of single U-slot and dual U-slot antenna", Antennas and Propagation Society, 2001 IEEE International Sym.

Volume: 2 , 2001, pp. 700 -703

[16] Lecture note from 24.427, "Antennas"

[17] J. R. James, and P. S. Hall, "Handbook of Microstrip Antennas", Vol. 1, 1989

[18] Yongxi Qian, and Itoh, T., " Planar periodic structures for microwave and millimeter wave circuit applications" Microwave Symposium Digest, 1999 IEEE MTT-S International , Vol. 4 , 1999, pp. 1533 -1536

[19] M. N. Mollah, and N. C. Karmakar, "Planar PBG structures and their applications to antenna", Antennas and Propagation Society, 2001 IEEE International Symp. , Vol. 2 , 2001, pp 494 -497

[20] B. Elamaran, Iao-Mak Chio, Liang-Yu Chen, and Jung-Chih Chiao, "A beam-steerer using reconfigurable PBG ground plane" Microwave Symposium Digest. 2000 IEEE MTT-S International, Vol. 2 , 2000, pp. 835 -838

[21] R. Coccioli, Deal, W.R., and T. Itoh, "Radiation characteristics of a patch antenna on a thin PBG substrate"Antennas and Propagation Society International Symposium, 1998. IEEE , Vol. 2 , 1998, pp. 656 -659

[22] T. Kim, and C. Seo, "A Novel Photonic Bandgap Structure for Low-Pass Filter of Wide Stopband", IEEE Microwave and Guided Wave Letters, Vol. 10, No. 1, Jan. 2000, pp. 13-15

[23] R. D. Meade, A. M. Rappe, and J. D. Joannopoulos, "Nature of photonic bandgap: some insights from a field analysis", J. Opt. Soc. Am. B/Vol. 10, No. 2, February 1993, pp. 328-332

[24] Fei-Ran Yang, Kuang-Ping Ma, Yongxi Qian, and T. Itoh, "A novel TEM waveguide using uniplanar compact photonic-bandgap (UC-PBG) structure", Microwave Theory and Techniques, IEEE Transactions on , Vol. 47 Issue: 11 , Nov. 1999 , pp. 2092 -2098

[25] M. Fallah-Rad, and L. Shafai, "Radiation Pattern Enhancement of Microstrip Patch Antennas Using A 2D Photonic Bandgap Structure", Symposium on Antenna Technology and Applied Electromagnetics, ANTEM 2002

[26] M. Fallah-Rad, and L. Shafai, "PARAMETRIC STUDY OF PBG GROUND PLANES IN MICROSTRIP TRANSMISSION LINES", Symposium on Antenna Technology and Applied Electromagnetics, ANTEM 2002

[27] M. Fallah-Rad, and L. Shafai, "EFFECTS OF GROUND PLANE PERFORATIONS ON THE PERFORMANCE OF MICROSTRIP PATCH ANTENNAS", Symposium on Antenna Technology and Applied Electromagnetics, ANTEM 2002

[28] Y. Qian, V. Radisic, and T. Itoh, "Simulation and Experiment of Photonic Band-Gap Structures for Microstrip Circuits", 1997 Asia Pacific Microwave Conference

[29] T. Y. Yun, and K. Chang, "Uniplanar One-Dimensional Photonic-Bandgap Structures and Resonator", IEEE Transactions on Microwave Theory and Technique, Vol. 49, No. 3, March 2001, pp. 549-553

[30] H. Y. D. Yang, "Theory of Microstrip Lines on Artificial Periodic Substrates", IEEE Transactions on Microwave Theory and Technique, Vol. 47, No. 5, May 1999 pp. 629-635

[31] R. C. Johnson, and H. Jasik, "Antenna Engineering Handbook", 2nd edition, McGraw Hill Book Company, 1984.

[32] S. Noghanian, and L. Shafai, "Control of microstrip antenna radiation characteristics by ground plane size and shape", Microwave, Antennas and Propagation, IEE proceedings, Vol. 45, Issue: 3, Jun. 1998 pp. 207-212